Divalent Cation Block and Competition between Divalent and Monovalent Cations in the Large-Conductance K^+ Channel from *Chara australis*

D. R. LAVER

From the Biophysics Laboratory, School of Biological Sciences, A12, The University of Sydney, New South Wales, 2006, Australia

ABSTRACT The patch-clamp technique is used to investigate divalent ion block of the large-conductance K^+ channel from *Chara australis*. Block by Ba^{2+}, Ca^{2+}, Mg^{2+}, and $Pt(NH_3)_4^{2+}$ from the vacuolar and cytoplasmic sides is used to probe the structure of, and ion interactions within, the pore. Five divalent ion binding sites are detected. Vacuolar Ca^{2+} reduces channel conductance by binding to a site located 7% along the membrane potential difference (site 1, $\delta = 0.07$; from the vacuolar side); it also causes channel closures with mean a duration of ~ 0.1–1 ms by binding at a deeper site (site 2, $\delta = 0.3$). Ca^{2+} can exit from site 2 into both the vacuolar and cytoplasmic solutions. Cytoplasmic Ca^{2+} reduces conductance by binding at two sites (site 3, $\delta = -0.21$; site 4, $\delta = -0.6$; from the cytoplasmic side) and causes closures with a mean duration of 10–100 ms by binding to site 5 ($\delta = -0.7$). The deep sites exhibit stronger ion specificity than the superficial sites. Cytoplasmic Ca^{2+} binds sequentially to sites 3–5 and Ca^{2+} at site 5 can be locked into the pore by a second Ca^{2+} at site 3 or 4. Ca^{2+} block is alleviated by increasing $[K^+]$ on the same side of the channel. Further, Ca^{2+} occupancy of the deep sites (2, 4, and 5) is reduced by K^+, Rb^+, NH_4^+, and Na^+ on the opposite side of the pore. Their relative efficacy correlates with their relative permeability in the channel. While some Ca^{2+} and K^+ sites compete for ions, Ca^{2+} and K^+ can simultaneously occupy the channel. Ca^{2+} binding at site 1 only partially blocks channel conduction. The results suggest the presence of four K^+ binding sites on the channel protein. One cytoplasmic facing site has an equilibrium affinity of 10 mM (site 6, $\delta = -0.3$) and one vacuolar site (site 7, $\delta < 0.2$) has low affinity (>500 mM). Divalent ion block of the *Chara* channel shows many similarities to that of the maxi-K channel from rat skeletal muscle.

INTRODUCTION

The K^+ permeation and gating properties of the large-conductance K^+ channel in the membrane surrounding cytoplasmic drops from *Chara australis* have been studied

Address reprint requests to Dr. D. R. Laver, Division of Neuroscience, John Curtin School of Medical Research, Australian National University, G.P.O. Box 334, Canberra, Australian Capital Territory, 2601, Australia.

J. GEN. PHYSIOL. © The Rockefeller University Press · 0022-1295/92/08/0269/32 $2.00
Volume 100 August 1992 269–300

in more detail than those of any other plant ion channel. The reason for this is that membrane-bound cytoplasmic drops are easily produced from *Chara* internodes. Their membrane readily forms robust high-resistance seals with patch-clamp pipettes which are stable over an enormous range of voltage. Further, the large conductance and high frequency of detection of this channel make it an ideal subject for detailed kinetic analysis.

The role of this channel in *Chara* has been postulated to be to regulate the flow of Ca^{2+} from the vacuole to the cytoplasm through voltage-dependent Ca^{2+} channels (Laver and Walker, 1991). However, its role is difficult to determine because the parent cell is disrupted during the production of cytoplasmic drops. Fluorescence labeling studies (Lühring, 1986; Sakano and Tazawa, 1986) show that part of the membrane delineating these drops is derived from the vacuolar membrane of the parent cell. With this in mind, the sidedness notation for the K^+ channel adopted in this paper is as follows: the side of the K^+ channel protein facing the cytoplasm in the cytoplasmic drop is called the cytoplasmic side and the other side is referred to as the vacuolar side.

The ion gating and permeation kinetics of this channel are complicated and in many respects are similar to those observed in large conductance K^+ (maxi-K) channels in animals (Laver and Walker, 1991). The channel has been shown to possess two voltage-dependent gates (Laver and Walker, 1987) and a Ca^{2+}-dependent gate (Laver and Walker, 1991) which causes the channel to be opened by micromolar cytosolic Ca^{2+}. As well as the open and closed states, the channel can also enter a variety of short-lived substates (Lühring, 1986; Tyerman, Terry, and Findlay, 1992); i.e., states associated with a smaller conductance than the main open state.

The K^+ permeation kinetics of this channel have so far been interpreted in terms of the following two models. Bertl (1989) used a cyclic kinetic model to explain K^+ permeation and its block by Na^+. In that model K^+ crosses the channel in one voltage-dependent step. The channel must then reset via a voltage-independent step before another K^+ can pass. Laver, Fairley, and Walker (1989) proposed a model where the channel presents a large number of uniform energy barriers to K^+ permeation. Further, permeation is assumed to be limited at high membrane potential difference (PD) by diffusion of ions near the pore mouths (i.e., diffusion limitation effect; Laüger [1976]) and at high $[K^+]$ by the maximum transport rate of the pore (described by Michaelis-Menten kinetics). Both models assume that ion conduction occurs by the interaction of only one ion at a time with the channel (single-ion conduction). However, there is considerable evidence for multi-ion conduction processes in K^+ channels from animal tissue. Further, a large-conductance K^+ channel from *Nitella* was shown to exhibit the "anomalous mole fraction" effect (Draber, Schultze, and Hansen, 1991), which is usually an indication of multi-ion kinetics. Draber et al. (1991) propose that two ions simultaneously interact with the channel protein. However, only one of these is believed to occupy the pore. The other is believed to bind at an external site away from the channel conduction pathway. This paper will examine again, more closely, the assumption of single-ion conduction in the *Chara* K^+ channel.

Neyton and Miller (1988*a*) made use of the interaction between Ba^{2+} and various monovalent cations to probe K^+ permeation within the maxi-K channel from rat

skeletal muscle. They found that the binding kinetics of Ba^{2+} were altered by the presence of K^+ in low concentrations. These results indicated the presence of two high-affinity K^+ binding sites located on each side of the channel protein. In their following paper (Neyton and Miller, 1988*b*) they found that monovalent cations could lock Ba^{2+} into the pore, indicating a further one or two lower affinity binding sites in the channel. They proposed that up to four K^+ ions can occupy the pore.

Divalent ions can also block K^+ permeation in the *Chara* channel from both sides of the cytoplasmic drop membrane (Laver, 1990; Laver and Walker, 1991). The blocking kinetics of Ca^{2+} on the vacuolar side has been studied in detail by Laver (1990). In that study it was found that Ca^{2+} reduced K^+ conductance and caused a "flicker block" (i.e., a train of blocking events that are of sufficient duration to be partially resolved by the recording apparatus). The Ca^{2+} block was analyzed within the framework of a theory of diffusion limitation of ion flow through pores (Laüger, 1976) and the Woodhull model of voltage-dependent ion block (Woodhull, 1973). The kinetics of the block revealed two binding sites located at 8 and 40% along the trans-pore PD and showed that the vestibule facing the vacuole cannot be occupied by more than one ion, Ca^{2+} or K^+.

The blocking characteristics of Ca^{2+} on the cytoplasmic side have also been measured (Laver and Walker, 1991) but were not studied in detail. In that study cytoplasmic Ca^{2+} was also found to block the channel in two ways, one that reduced the channel conductance and the other that caused long channel closures.

This study investigates in greater detail the block by Ca^{2+} on the cytoplasmic side of the large-conductance K^+ channel in *Chara*. It adopts the approach taken by Neyton and Miller (1988*a*, *b*) to investigate the possibility of simultaneous occupancy of the pore by several ions, to elucidate their interactions within the channel, and so to provide a basis on which to develop multi-ion models for ion permeation. The Ca^{2+} blocking kinetics on the *Chara* K^+ channel in the presence of monovalent cations is described to compare the mechanisms in channels from plants and animals.

Block by some other group IIa cations has been studied to further probe the various ion binding sites on the channel protein. Tetra-amine-platinum (II) ($Pt(NH_3)_4^{2+}$) has a square planar structure with an anhydrous radius of ~ 0.35 nm. The binding kinetics of this large cation yields additional clues about the local environment of the divalent ion sites on the protein.

MATERIALS AND METHODS

Experimental Protocol

Cytoplasmic drops were formed from internodal cells of *Chara australis* R. Br. using the method of Kamiya and Kuroda (1957). During experiments the bathing solution for the cytoplasmic drops contained either 150 or 500 mM alkali chloride solution plus a minimum of 0.1 mM $CaCl_2$ to stabilize the drop membrane. Measurements were carried out over 20–23°C. All measurements were adjusted to that expected at 23°C using a value of the Q_{10} for conductance of 1.3 (Laver, D.R., unpublished data).

Ca^{2+}, Ba^{2+}, and Mg^{2+} were added to solutions as chloride salts and $Pt(NH_3)_4^{2+}$ ions were added as $Pt(NH_3)_4(ClO_4)_2$ (from Dr. J. Beattie, School of chemistry, The University of Sydney, Sydney, Australia). During studies of channel gating cytosolic [Ca^{2+}] was kept >0.1 mM in

order to keep the Ca^{2+}-dependent gate open. Channel closures due to the Ca^{2+}-dependent gate would otherwise confuse the interpretation of the Ca^{2+}-dependent slow blocking kinetics.

Details of the patch pipette fabrication and recording and display apparatus have been described previously by Laver and Walker (1987) and Laver et al. (1989). Micropipettes were made from borosilicate glass with an internally fused microfilament (Bioscience No. 5512). Inside-out patches were formed by sealing (seal resistance varied from 10 to 50 GΩ) fire-polished pipette electrodes with the cytoplasmic drop membrane and then separating the pipette from the cytoplasmic drop. Occasionally when the membrane would form a vesicle on the pipette tip it was possible to get inside-out patches by briefly exposing the patch to air. Because of the known asymmetry in the voltage-dependent kinetics of the channel it was clear that these were in fact inside-out patches.

Presumably the side of the membrane that faces the cytoplasm in the intact cell (the inside face) also faces the cytoplasmic interior of the drop. The membrane PD is defined with respect to the vacuolar side (the outside of the drop) of the membrane as zero. Positive transmembrane current indicates positive charge flowing from the inside of the membrane.

During measurements of the stationary gating kinetics of the K^+ channel the pipette potential was clamped to a random sequence of values over the range ±300 mV for periods of 10–100 s. As the membrane PD increases beyond ±200 mV, the lifetime of the membrane patches decreases so that at 300 mV the patch rarely lasts longer than a few seconds. Hence excursions to large membrane PDs were kept as brief as possible. Measurements of unitary currents were carried out on patches where the pipette potential was slowly varied (manually) over the desired voltage range. The signal to noise ratio of the recordings was improved several-fold by holding the excised membrane patches just below the surface of the bath. The time course of the pipette current and voltage were recorded simultaneously on videotape using pulse code modulation (PCM-501; Sony Corp.) with a sampling rate of 44 kHz. Current signals were recorded with a bandwidth of 10 kHz. Theory was fitted with data using a least-squares routine. The errors quoted here represent 95% confidence limits.

Measurement of Rapid Blocking Kinetics

The analysis of the blocking kinetics of divalent cations was done using ion activities rather than concentrations. Ionic activity coefficients, τ, were estimated using the Gouy-Chapman "limiting law" (Margolis, 1966):

$$-\log \tau = \frac{0.509 z^2 \mu^{1/2}}{1 + \mu^{1/2}} \tag{1}$$

μ is the ionic strength of the solution and z is the valency of the ion. The activity coefficients for divalent ions at concentrations used in these experiments are commonly as low as 0.1. This should be remembered when comparing binding parameters derived here with others that have been derived using ion concentrations.

The attenuating effect of divalent cations upon the K^+ channel unitary current is presumably the time average of binding events that are too rapid to be resolved by the recording apparatus. Provided ion binding completely blocks the channel, then the probability they are bound, P, can be determined from the ratio of the unitary currents in their presence, $I(X^{2+})$, and absence, I^0:

$$1 - P = I(X^{2+})/I^0 \tag{2}$$

Analysis of patch recordings for unitary current amplitudes was done in one of two ways. Either the manual approach (e.g., Laver et al., 1989) was used in which unitary current steps

were measured directly from their time course as displayed on a CRO or a new automated technique was used for detecting current transitions.

The automated method used here is based on a technique for analyzing current transitions in multi-level single channel recordings (Vivaudou, Singer, and Walsh, 1986). The analysis of the current records is done in two passes. The first pass compacts the data and the second discriminates the channel signal from background noise and digitizing artifacts. The main difference between the method used here and that used by Vivaudou et al. (1986) is that no attempt is made here to determine the state (i.e., number of simultaneously open channels) of the patch. The current and voltage recordings are both analyzed together so that the magnitude of channel current transitions can be correlated with the membrane PD. The voltage dependence of all current transitions (including background noise) is displayed on a two-dimensional, color-contoured frequency distribution. The automated method was found to be particularly useful when several types of channels were present in a patch where with manual detection techniques it was easy to confuse current steps associated with different channel types.

Interpretation of the association rate of the blocking ion in terms of binding site properties is dependent on the specific model chosen for K^+ permeation within the pore. For rapid blocking kinetics the binding and unbinding steps cannot be analyzed separately because of the limited bandwidth of the recording apparatus. The problem is, however, that this study aims to identify the overall characteristics of the K^+ permeation in order to develop such a model. To cope with this dilemma this study will avoid as much as possible the use of specific K^+ permeation models in analyzing rapid blocking kinetics. Consequently, fundamental binding site parameters such as affinity cannot be derived from empirical constants such as concentration of half-inhibition.

Measurement of Slow Ca^{2+} Blocking Kinetics

Ca^{2+} also binds to the channel protein on the millisecond time scale. Here individual binding events can be observed directly by measuring the Ca^{2+}-induced gating of the K^+ current. The protocol for measuring the K^+ channel gating events has been elaborated by Laver and Walker (1987). Briefly, frequency distributions of open and closed durations were compiled from single channel recordings using the software package IPROC2 (from Dr C. Lingle, Department of Biological Sciences, Florida State University, Tallahassee, FL).

Analysis of slow blocking kinetics "flicker block" of vacuolar 20 mM Ca^{2+} has been done in an earlier study (Laver, 1990). The block becomes quite apparent as the membrane PD becomes more negative than −150 mV. At these PDs the block is manifest as a 10-fold reduction in the mean open time of the channel and a 10-fold increase in relative frequency of observed short closures ($t < 1$ ms) in the closed duration frequency distributions. Thus 90% of the channel closures are Ca^{2+} induced and so reflect blocking events. Therefore, under these conditions the reciprocal of the mean open and closed durations give a good estimate of the Ca^{2+} association (k_{on}) and dissociation rates (k_{off}) with the channel protein from the vacuolar side. In calculating k_{off} and k_{on} allowance was made for unresolved events using the method of Blatz and Magleby (1986).

The slow block by cytoplasmic Ca^{2+} has not previously been studied in detail. However, it appears that the kinetics of Ca^{2+} binding is at least an order of magnitude slower than that of vacuolar Ca^{2+} (Laver and Walker, 1991). In this case only a small fraction of the channel gating is Ca^{2+} induced. However, these closures are easily recognized because they have relatively long durations which cause channel activity to be separated into bursts. The durations of the observed bursts and gaps between these bursts are interpreted as intervals where Ca^{2+} is either unbound or bound to the channel. Because it is not possible to identify which individual closures are due to Ca^{2+} binding, they are defined here as shut intervals that exceed a threshold duration. The threshold duration is set so that at least 90% of the closures exceeding the threshold are due to blocking events. This is determined from frequency distributions of

channel closures in the presence and absence of Ca^{2+}. The threshold values so determined vary with membrane PD and $[Ca^{2+}]$ over the range 5–50 ms. Association and dissociation constants could then be derived from the burst, gap, and threshold durations using the method of Blatz and Magleby (1986).

RESULTS

The effects of vacuolar and cytosolic Ca^{2+} on the time course of the K^+ channel unitary current are shown in Fig. 1. The current–voltage characteristics in both the

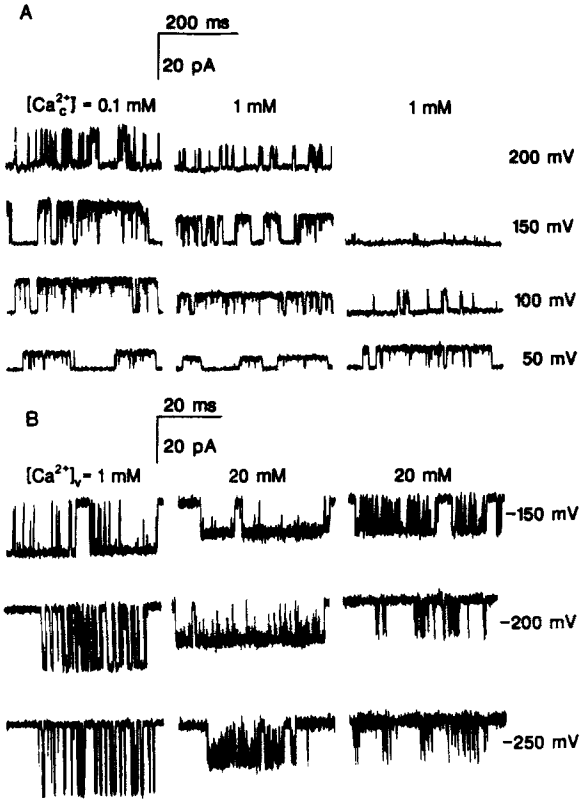

FIGURE 1. The effect of Ca^{2+} on the time course of unitary currents through the large-conductance K^+ channel in excised membrane patches at several membrane PDs. (*A*) The effects of vacuolar Ca^{2+} in both the presence and absence of K^+ in the cytoplasmic solution. The vacuolar solution contains 150 mM KCl. The cytoplasmic solutions contain (*1*) 150 mM NaCl; (*2*) 500 mM KCl; (*3*) 150 mM NaCl. The current baseline is toward the top of each trace and the data are filtered at 10 kHz. Ca^{2+} decreases the unitary current steps and causes brief channel closures. The mean duration of these closures is longer in the absence of cytoplasmic K^+. (*B*) The effects of cytoplasmic Ca^{2+} in both the presence and absence of K^+ in the vacuolar solution. The cytoplasmic solution contains 150 mM KCl. The vacuolar solutions contain (*1*) 150 mM KCl; (*2*) 150 mM KCl; (*3*) 150 mM NaCl. The current baseline is toward the bottom of each trace and the data are filtered at 1.25 kHz. Ca^{2+} both decreases the unitary current and causes channel closures. Vacuolar K^+ affects both forms of the Ca^{2+} block.

presence and absence of Ca^{2+} have been shown in previous publications (Laver et al., 1989; Laver, 1990; Laver and Walker, 1991); none are shown here. The results are compared with predictions of a model that assumes that divalent and monovalent cations bind to saturable sites (labeled 1–7) on the channel protein. A summary of the main features of these sites is given in Table I.

TABLE I

A Summary of the Kinetic Properties and Ion Binding Sites on the K⁺ Channel Protein and How They Were Determined from This Study

Site No.	δ		Binding parameters K_I or K_D (mM) at 0 mV					Experimental verification
1								
Divalent	0.07		K_{I1} independent of $[K^+]_c$					Reduced current at
Vacuolar			$Pt(NH_3)_4^{2+} > Ba^{2+} > Mg^{2+} > Ca^{2+}$					negative PDs;
Fast block			10	14	28	32		Figs. 1–3
2								
Divalent	0.3		K_{I2} depends on $[K^+]_c$					Ion-induced closures
Vacuolar			$Ba^{2+} > Ca^{2+} > Pt(NH_3)_4^{2+}$					(0.1–1 ms)
Slow block		(a)	0.5	290	$>10^4$			at negative PDs;
								Figs. 1, 4–6
3								
Divalent	−0.21		K_{I3} depends weakly on $[K^+]_v$					Reduced current at
Cytoplasmic			$Ba^{2+} > Mg^{2+}, Sr^{2+} > Pt(NH_3)_4^{2+} > Ca^{2+}$					positive PDs;
Fast block		(b)	3.8	8	8	9	11.8	Figs. 1, 7–10
		(c)	–	6	–	5.2	8	
4								
Divalent	−0.6		K_{I4} depends strongly on $[K^+]_v$					Reduced current
Cytoplasmic			$Ca^{2+} > Pt(NH_3)_4^{2+}, Mg^{2+}$					at positive PDs;
Fast block		(c)	73	>1,000	>1,000			Figs. 1, 7, 9, 10
5								
Divalent	−0.7		K_{I5} depends strongly on $[K^+]_v$					Ion-induced long
Cytoplasmic			$Ba^{2+} > Sr^{2+} > Ca^{2+} > Mg^{2+} > Pt(NH_3)_4^{2+}$					closures (10–100 ms)
Slow block		(b)	1.2	47	10^4	4.7×10^4	$<2 \times 10^4$	at positive PDs;
								Figs. 1, 12, 13
6								
Monovalent	−0.3		K_{D6}					K_{I2} and k^2_{off} depend
Cytoplasmic			$K^+ > Rb^+ > NH_4^+ > Na^+$					on cytoplasmic
			10	77	210	>400		monovalent cation
								concentration;
								Figs. 1, 5, 6
7								
Monovalent	<0.2		K_{D7} is not well determined					K_{I5}, k^5_{off}, and k^5_{on} depend
Vacuolar			$K^+ > Rb^+ > NH_4^+ > Na^+$					on vacuolar
								cation
								concentration; Fig. 14

δ is the fraction of the transmembrane PD between the binding site and vacuolar (positive value) or cytoplasmic (negative value) sides of the membrane. (*a*) $[K^+]_c$ = 0 mM; (*b*) $[K^+]_v$ = 150 mM; (*c*) $[K^+]_v$ = 0 mM.

Rapid Block from the Vacuolar Side

Figs. 2–6 illustrate the blocking kinetics of vacuolar Ca^{2+}. Fig. 2 shows the attenuating action of Ca^{2+}, Mg^{2+}, Ba^{2+}, and $Pt(NH_3)_4^{2+}$ inside the pipette on the channel current in excised inside-out patches. Their block is weakly voltage dependent and has a hyperbolic dependence on concentration (Fig. 3). Competition between Ca^{2+} and K^+ was investigated by measuring the blocking effect of Ca^{2+} over a wide range of vacuolar $[K^+]$. These results show that there is a small component of the current

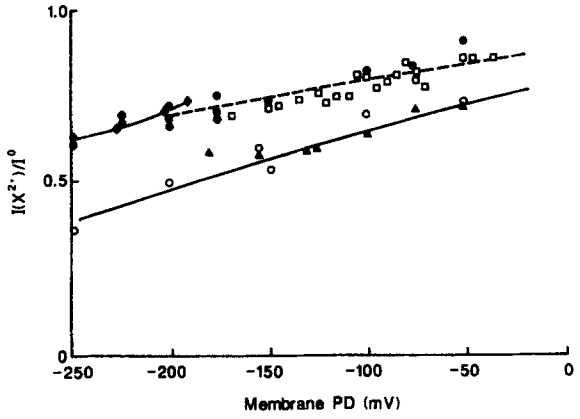

FIGURE 2. The attenuation of the K^+ channel unitary current in excised inside-out patches by divalent cations in the pipette. The block is presented here as the ratio of the unitary current in the presence of divalent cations, I, and the control, I^0, (in the absence of vacuolar $[X^{2+}]$). With 150 mM KCl (cytoplasmic side) in the bath and the pipette (vacuolar side), the vacuolar divalent ion concentrations were 20 mM Ca^{2+} (●), 20 mM Mg^{2+} (□), 20 mM Ba^{2+} (▲), and 10 mM $Pt(NH_3)_4^{2+}$ (○). With 150 mM KCl in the pipette and 150 NaCl in the bath, the concentration was 20 mM Ca^{2+} (◆). The lines show solutions to Eqs. 3 and 4. The parameters for the full line are K_I (0) = 30 mM and δ_1 = 0.07 ($[X^{2+}]$ = 20 mM and activity coefficient, $\tau_{X^{2+}}$ = 0.23) and for the dashed line K_I (0) = 10 mM and δ_1 = 0.09 ($[X^{2+}]$ = 10 mM and τ_{K^+} = 0.24). B is assumed to be zero, which is a reasonable approximation at these ion concentrations (see Discussion).

that is not inhibited by Ca^{2+}. This component amounts to ~1 pA at a membrane PD of −150 mV when [KCl] = 10 mM. This violates the assumptions used in deriving Eq. 2 so that $I(Ca^{2+})/I^0$ cannot be used to measure the binding probability of the blocking ion using this equation. However, because the noninhibited component of the current is relatively small, Eq. 3 provides a good approximation for the activity of half inhibition, K_{I1}:

$$I(X^{2+})/I^0 = (1 - B)(1 + a_X/K_{I1})^{-1} + B \tag{3}$$

where a_X is the vacuolar activity of divalent ion species X^{2+}, and B represents the noninhibited component of channel conduction. According to the Woodhull model

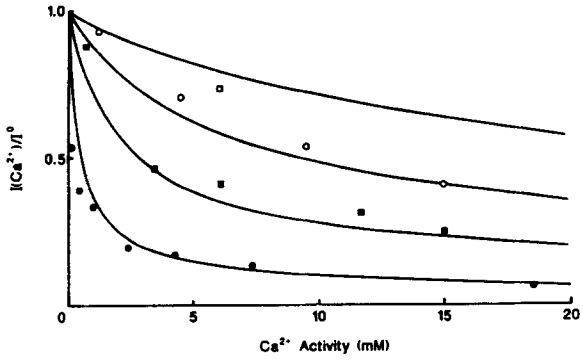

FIGURE 3. Block by vacuolar Ca^{2+} of K^+ channel current over a range of vacuolar [KCl] at a membrane PD of −150 mV. The cytoplasmic solution contained 150 mM NaCl and 5 mM $CaCl_2$. The solid lines are the prediction of a multi-ion binding model (see Scheme 2 and Eqs. 18 and 19) for which the pore is assumed to conduct K^+ even in the presence of bound Ca^{2+}. The KCl concentrations are 10 mM, τ_{K^+} = 0.9 (●), 50 mM, τ_{K^+} = 0.74 (■), 150 mM, τ_{K^+} = 0.66 (○), and 500 mM, τ_{K^+} = 0.64 (□). The parameters of the fit are: K_{DK} = 0.79 mM, K_{D2K} = 100 mM, K_{DCa} = 0.05 mM, K_{DKCa} = 100 mM, I_K = 30 pA, I_{KCa} = 20 pA, and I_{2K} = 100 pA.

(Woodhull, 1973) the voltage dependence of K_{I1} is given by:

$$K_{I1}(V) = K_{I1}(0) \exp(\delta_1 zFV/RT) \quad (4)$$

where δ_1 is the fraction of the membrane PD, V (the electrical distance), between the divalent ion binding site (site 1) and the vacuolar solution. Eqs. 3 and 4 are fitted with the data in Figs. 2 and 3 (fits not shown).

$K_{I1}(0)$ for Ca^{2+} increases with increasing vacuolar $[K^+]$ and $[Na^+]$ from 0.5 ± 0.1 mM in 10 mM KCl to 32 ± 2 mM in 150 mM KCl, 42 ± 3 mM in 500 mM KCl, and 64 ± 20 mM in 150 mM KCl + 350 mM NaCl. Theoretical fits to the data in Fig. 2

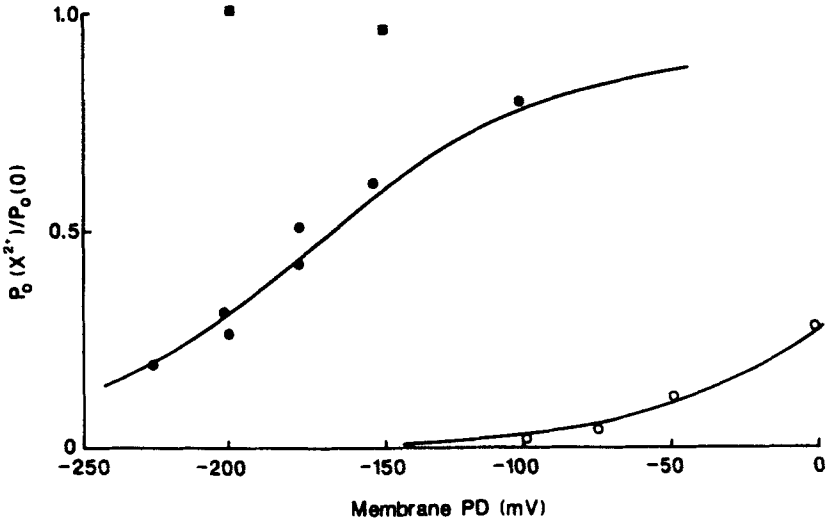

FIGURE 4. The slow block of the channel measured by the relative open probability in the presence of divalent cations in the vacuolar solution. This is derived from the ratio of the open probability of the blocked channel with that of the channel at low divalent ion concentrations. The vacuolar solution (pipette) contained 150 mM KCl and the following concentrations of divalent ions: 20 mM Ca^{2+}, $\tau_{Ca^{2+}}$ = 0.22 (●), 4 mM Ba^{2+}, $\tau_{Ba^{2+}}$ = 0.26 (○), 10 mM Pt $(NH_3)_4^{2+}$, $\tau_{Pt(NH_3)_4^{2+}}$ = 0.25 (■). The cytoplasmic solution (bath) contained 150 mM NaCl. The solid lines are fits to the data by Eqs. 5 and 6. The parameters of the fits are: Ba^{2+}, K_{I2} (0) = (0.5 ± 0.1) mM, δ_2 = 0.3; Ca^{2+}, K_{I2} (0) = (290 ± 30) mM, δ_2 = 0.3 ± 0.01. δ_2 for Ba^{2+} is assumed to be the same as for Ca^{2+}.

give δ_1 = 0.07 ± 0.02, which is the same as that found previously (Laver, 1990). Exchanging KCl for NaCl on the cytoplasmic side had no effect on Ca^{2+} block.

Applying this analysis to block by other divalent cations, it was found that this site discriminates poorly between divalent ions, the binding sequence being ($K_{I1}(0)$): $Pt(NH_3)_4^{2+}$ (10 ± 1 mM) > Ba^{2+} (14 ± 2 mM) > Mg^{2+} (28 ± 2 mM) > Ca^{2+} (32 ± 2 mM).

Slow Block from the Vacuolar Side

The inhibitory effect of the slow blocking kinetics of Ba^{2+}, Ca^{2+}, and $Pt(NH_3)_4^{2+}$ is shown in Fig. 4. The block is represented by the open probability, P_o, of the channel

relative to that in the absence of divalent ions on the vacuolar side. The data are fitted with Eqs. 5 and 6:

$$P_o(X^{2+})/P_o(0) = (1 + a_X/K_{I2})^{-1} \quad (5)$$

$$K_{I2}(V) = K_{I2}(0) \exp(\delta_2 zFV/RT) \quad (6)$$

The voltage dependence of the block ($\delta_2 = 0.3 \pm 0.01$) is stronger than that for site 1. The binding affinity sequence, represented by $K_{I2}(0)$ of site 2 is: Ba^{2+} (0.5 ± 0.1 mM) > Ca^{2+} (290 ± 30 mM) > $Pt(NH_3)_4^{2+}$ (> 10 M).

Because the Ca^{2+} blocking events are long enough to be resolved by the recording apparatus, the channel conductance in the Ca^{2+} blocked state can be measured directly. The conductance of the blocked channel could not be resolved from the baseline and so was found to be < 1% of the open channel conductance.

The Ca^{2+} association (k_{on}^2) and dissociation (k_{off}^2) rates derived from the Ca^{2+}-induced closures (see Materials and Methods) are shown in Fig. 5. Under conditions of high ionic strength in the cytoplasmic solution the voltage dependences of k_{on}^2 and k_{off}^2 can be described by single exponentials that have opposite voltage dependences of approximately equal magnitude. This suggests that when Ca^{2+} dissociates from site 2 it returns to the vacuolar solution. However, at low ionic strength when the cytoplasmic solution contains only 2 mM $CaCl_2$ k_{off}^2 cannot be described by a single exponential. The data were then fitted with the sum of two exponentials reflecting two Ca^{2+} dissociation processes:

$$k_{off}^2 = k_1^2 \exp(\delta_2 zFV/2RT) + k_2^2 \exp(\delta_{2a} zFV/2RT) \quad (7)$$

The parameters of the fit are: $\delta_2 = 0.9 \pm 0.25$, $\delta_{2a} = -0.15 \pm 0.15$, $k_1^2 = (5.7 \pm 3.9)\cdot 10^4\ s^{-1}$, and $k_2^2 = (3 \pm 3)\cdot 10^2\ s^{-1}$. The first exponential term reflects the dissociation back to the vacuolar solution. The voltage dependence of the second exponential component, being opposite to that of the first, indicates Ca^{2+} dissociation to the cytoplasmic solution.

Competition between Ca^{2+} and K^+ within the pore was studied by the effect of $[K^+]$ on both sides of the channel on Ca^{2+} block at high ionic strength. It is found that k_{on}^2 is reduced by increasing vacuolar [KCl] (result not shown) and is also unaffected by exchanging Na^+ for K^+ on the cytoplasmic side. The k_{off}^2, on the other hand, could be reduced sixfold by replacing cytoplasmic 150 mM KCl with NaCl. The effects of K^+, Rb^+, NH_4^+, and Na^+ on k_{off}^2 are shown in more detail in Fig. 6, where it can be seen that k_{off}^2 follows a hyperbolic dependence on vacuolar $[K^+]$. These data are fitted with Eqs. 8–10, where the $[K^+]$-induced change in k_{off}^2 is related to the occupancy of a K^+ site facing the cytoplasmic side (site 6):

$$k_{off}^2(a_K, V) = k_{off}^2(\infty, V)(1 + K_{D6}/a_K)^{-1} + k_{off}^2(0, V) \quad (8)$$

where a_K is the cytoplasmic K^+ activity and K_{D6} is the K^+ dissociation constant. The voltage dependences of K_{D6} and k_{off}^2 at $a_K = 0$ and ∞ are given by:

$$K_{D6}(V) = K_{D6}(0) \exp(\delta_6 zFV/RT) \quad (9)$$

$$k_{off}^2(i, V) = k_{off}^2(i, 0) \exp(\delta_2 zFV/2RT); \qquad i = 0 \text{ or } \infty \quad (10)$$

where δ_6 is the electrical distance of the K^+ site from the cytoplasmic side of the pore (i.e., δ_6 is negative) and δ_2 is that of the Ca^{2+} site from the vacuolar side. In deriving Eq. 10 it is assumed that energy barriers to Ca^{2+} binding are symmetric.

The value of K_{D6} depends on the membrane PD ($\delta_6 = -0.30 \pm 0.10$) and the ion species in the cytoplasmic solution. For K^+ binding $K_{D6}(0) = 10 \pm 7$ mM and K_{D6} varies from 100 mM at −175 mV to 240 mM at −250 mV. Cytoplasmic Na^+ at

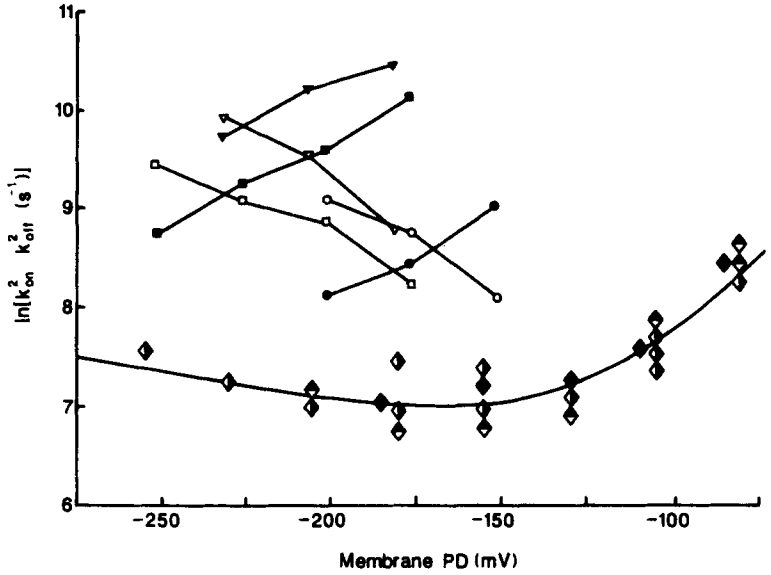

FIGURE 5. The Ca^{2+} dissociation, k^2_{off} (*filled symbols*) and association rates, k^2_{on} (*open symbols*), derived from the slow block induced by vacuolar Ca^{2+}. The data are corrected to allow for unresolved events using the method of Blatz and Magleby (1986). The dead time of the system (i.e., the shortest detectable event duration) when filtering the single channel recordings at 10 kHz was measured to be 35 μs. The vacuolar solution contained 20 mM $CaCl_2$ and 150 mM KCl. The ion concentrations (mM) of various cytoplasmic solutions are 150 NaCl (*circles*), 80 KCl + 70 NaCl (*squares*), and 150 KCl (*triangles*). k^2_{off} at low cytosolic ionic strength is also shown where the cytosolic solutions contained 2 mM $CaCl_2$ plus nonelectrolyte osmoticants. These are indicated by the points (◆) none; (◆) 300 mM sucrose; and (◆) 300 mM manitol. Data joined by lines are from the same patches. The association rate shows no significant dependence on cytoplasmic [KCl]. However, the dissociation rate is increased by increasing cytoplasmic [KCl]. The solid curve shows a fit of two exponentials (Eq. 7) to k^2_{off}. The parameters of the fit to k^2_{off} are: $\delta_2 = 0.9 \pm 0.25$, $\delta_{2a} = -0.15 \pm 0.15$, $k^2_1 = (5.7 \pm 3.9)\cdot10^4\ s^{-1}$, $k^2_2 = (3 \pm 4)\cdot10^2\ s^{-1}$. The parameters of the fit to k^2_{on} are: $\delta_2 = 0.5 \pm 0.05$, $k^2_{on}(0) = (2.7 \pm 0.3)\cdot10^2\ s^{-1}$.

concentrations up to 500 mM had no significant effect on k^2_{off}. The voltage dependence of the dissociation rate ($\delta_2 = 0.3 \pm 0.07$) is similar to that found previously by Laver (1990). Cytoplasmic K^+ increases k^2_{off}(0 mV) from $(3.0 \pm 1.0)\cdot10^4$ s^{-1} at low concentrations to an upper limit of $(4.0 \pm 0.05)\cdot10^5\ s^{-1}$ at high concentrations. K_{D6} (−200 mV) for binding of monovalent cations is: K^+ (131 ± 30 mM) > Rb^+ (850 mM) > NH_4^+ (2.3 M) > Na^+ (>4 M).

Rapid Block from the Cytoplasmic Side

The results shown in Figs. 7–11 show the rapid block induced by divalent cations on the cytoplasmic side. The characteristics of cytoplasmic Ca^{2+} block are more complicated than those found for vacuolar Ca^{2+}. To distinguish between the various components of the block, the effect of divalent ions on the unitary current was measured in the presence and absence of K^+ in the vacuolar solution. Fig. 7 shows the block by Ca^{2+} and $Pt(NH_3)_4^{2+}$ plotted on a scale that represents binding at a single site (Woodhull model) as a straight line. Deviation from a single site model is most clearly evident for the Ca^{2+} block at low vacuolar [K^+]. It is possible that there are two binding sites associated with the rapid kinetics and that Ca^{2+} binding at one of the sites is only significant at low vacuolar [K^+]. To further investigate this

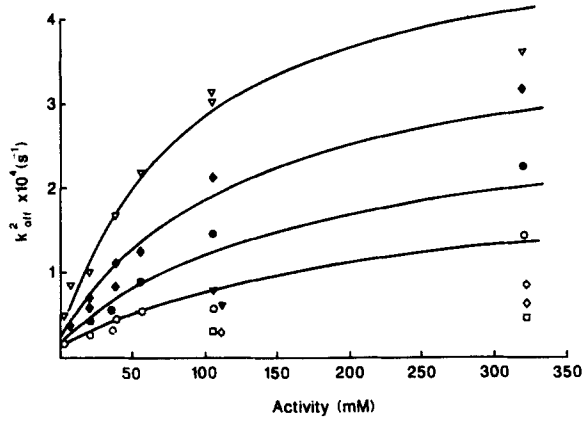

FIGURE 6. The Ca^{2+} dissociation rate k^2_{off} at four membrane PDs measured from the vacuolar Ca^{2+}-induced slow block is plotted against the activity of various monovalent cations in the cytoplasmic solution. Where possible, the ionic strengths of the cytoplasmic solutions were made up to 150 mM by adding NaCl. The data showing the effect of cytoplasmic K^+ are (symbol, membrane PD): (▽) −175 mV, (◆) −200 mV, (●) −225 mV, and (○) −250 mV. Data showing the effect of other cations at a membrane PD of −200 mV are: (▼) Rb^+, (◇) NH_4^+, and (□) Na^+. The solid curves are fits of Eqs. 8–10 to the K^+ data. The parameters of the fit are $K_{D6}(0)$ = (9.5 ± 7) mM, δ_6 = −0.3 ± 0.10, $k^2_{off}(a_K = 0, 0\text{ mV})$ = (3.0 ± 1.0) × 10^4 s^{-1}, $k^2_{off}(a_K = \infty, 0\text{ mV})$ = (4.0 ± 0.5) × 10^5 s^{-1}, δ_2 = 0.3 ± 0.07. For the other monovalent cations $K_{D6}(0)$ was calculated by using a value of $k^2_{off}(a_K = \infty, 0\text{ mV})$ = (4.0 ± 0.5) × 10^5 s^{-1}. Values of K_{D6} are: Rb^+, 63 mM; NH_4^+, 170 mM; Na^+, >330 mM.

possibility the data in Figs. 8–10 were fitted with either Eq. 11 or 12, from which the properties of two divalent cation sites facing the cytoplasmic side (sites 3 and 4) can be resolved.

If divalent ions at either site 3 or 4 totally block the pore, then for the case when these sites compete for ions,

$$I(X^{2+})/I^0 = (1 + a_X/K_{I3} + a_X/K_{I4})^{-1} \quad (11)$$

where a_X is the cytoplasmic activity of X^{2+} and K_{I3} and K_{I4} are half-inhibition constants associated with each site. Alternatively, if ions can bind independently at both sites (noncompetitive model):

$$I(X^{2+})/I^0 = [(1 + a_X/K_{I3})(1 + a_X/K_{I4})]^{-1} \quad (12)$$

The electrical distances of these sites (δ_3 and δ_4) from the cytoplasmic side are related to the voltage dependences of K_{I3} and K_{I4} by an equation similar to Eq. 6.

Fig. 8 shows the blocking effect of Ca^{2+} in the presence of 500 mM KCl on both sides of the membrane. Under these conditions Ca^{2+} blocked the channel as though binding to a single saturable site where $K_{I4}(0) \sim \infty$, $\delta_3 = -0.21 \pm 0.02$, and $K_{I3}(0)$ increases with increasing cytoplasmic $[K^+]$ from 11.8 ± 0.4 mM in 150 mM KCl to 23 ± 1 mM in 500 mM KCl (cf. Figs. 9 and 10).

Fig. 9 shows the block by cytoplasmic 1 mM Ca^{2+} in the presence of various monovalent cations in the vacuolar solution. The findings are that the varying ionic strength of the vacuolar solution from 150 to 3 mM (at constant $[K^+]$) had no effect on the Ca^{2+} block. However, the block is dependent on the ionic species present.

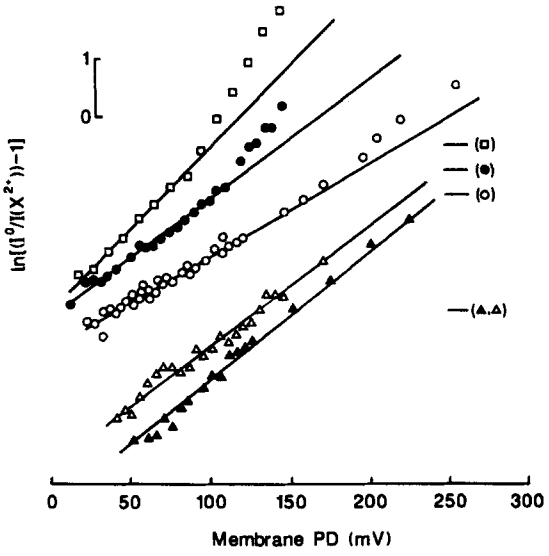

FIGURE 7. Attenuation of unitary channel current by divalent ions in the cytoplasmic solution. The data for Ca^{2+} block in the presence of cytoplasmic 500 mM KCl are shown where the vacuolar solutions contain 500 mM NaCl (□), 3 mM KCl, 500 mM NaCl (●), and 500 mM KCl (○). The data show the $Pt(NH_3)_4^{2+}$ block in the presence of cytoplasmic 150 mM KCl where the cytoplasmic solutions contain 150 mM KCl (▲) and 150 mM NaCl (△). The current is plotted in such a way as to show more clearly the multi-exponential voltage dependence of Ca^{2+} binding. The data have been displaced along the vertical axis for clarity. The horizontal bars indicate the zero associated with each data set. On these axes Eqs. 11 and 12, which describe binding at a single site, appear as straight lines; this is the case for $Pt(NH_3)_4^{2+}$. Deviations of the Ca^{2+} data from a straight line reflect binding at more than one site within the pore. The straight lines are fits to the data at membrane PDs < 100 mV.

When vacuolar KCl is exchanged for NaCl the block by cytoplasmic Ca^{2+} is enhanced at more positive membrane PDs (e.g., see Figs. 9 *B* and 10 *A*). The enhanced block also has a stronger voltage dependence. In terms of either Eq. 11 or 12 this corresponds to a large decrease in K_{I4} and a 30–70% decrease in K_{I3}. Under these conditions the block is dominated by the kinetics of Ca^{2+} binding at site 4, where $\delta_4 = -0.6 \pm 0.05$ and $K_{I4}(0)$ (at zero vacuolar $[K^+]$) increases with increasing cytoplasmic $[K^+]$ from (50 ± 6) mM at 150 mM KCl to (214 ± 17) mM at 500 mM KCl.

Fig. 10 shows the effect of vacuolar $[K^+]$ on block by 10 mM cytoplasmic Ca^{2+}, Mg^{2+}, and 1 mM $Pt(NH_3)_4^{2+}$. For Mg^{2+} and $Pt(NH_3)_4^{2+}$ the removal of vacuolar K^+ does not introduce an additional exponential component to the voltage-dependent

block as it does for Ca^{2+} (also see Fig. 7). Hence the relatively small effect of vacuolar K^+ on ion binding at site 3 can be seen most clearly from the Mg^{2+} and $Pt(NH_3)_4^{2+}$ data.

A comparison of the predictions of the competitive and noncompetitive binding models (i.e., Eqs. 11 and 12) is shown in Fig. 9 *B*. It was found that Eq. 11 always gave a better fit to the data than Eq. 12. The noncompetitive model (Eq. 12) predicts a maximum in the voltage dependence of Ca^{2+} block at intermediate vacuolar [K^+] which is not apparent in the data. Hence the binding parameters presented here are derived from the competitive model (Eq. 11).

The inhibition constants for Mg^{2+}, Ca^{2+}, and $Pt(NH_3)_4^{2+}$ are derived from the data in Fig. 10 *B* by fitting the data with Eq. 11. The binding sequence, $K_{I3}(0)$ (millimolar),

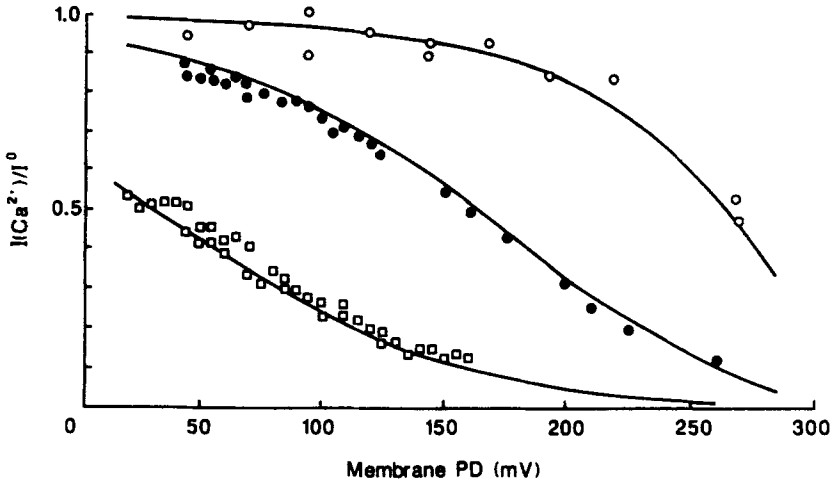

FIGURE 8. The attenuation of the K^+ channel unitary current in excised inside-out patches by three concentrations of cytoplasmic Ca^{2+} (in the bath). These are: 1 mM (○), 10 mM (●), and 100 mM (□). The solutions on each side of the patch contain 500 mM KCl. The control current (I^0) was measured from patches in the presence of <0.1 mM cytoplasmic $CaCl_2$. The solid lines show the least-squares fit of Eq. 11 with the data. The parameters of the fit are: $K_{I4}(0) = \infty$, $K_{I3}(0) = (23 \pm 1)$ mM, $\delta_3 = -0.21 \pm 0.02$. The range of values for the ion activity coeffients used in the analysis are $\tau_{K+} = 0.57$–0.61 and $\tau_{Ca^{2+}} = 0.11$–0.14. The model fit indicated that the blocking characteristics shown here are dominated by the blocking kinetics of site 3.

of site 3 in cytoplasmic 150 mM KCl in the presence and absence of vacuolar 150 mM K^+ is: Ba^{2+} (3.8 ± 1;—), Mg^{2+} (8 ± 1; 6 ± 1), Sr^{2+} (8 ± 1;—), $Pt(NH_3)_4^{2+}$ (9 ± 1; 5.2 ± 0.5), Ca^{2+} (11.8 ± 0.4; 8 ± 2). The data for Ba^{2+} and Sr^{2+} block have been taken from Laver and Walker (1991). The binding sequence for site 4 in the absence of vacuolar K^+ is: Ca^{2+} (73 ± 5 mM) > $Pt(NH_3)_4^{2+}$ and Mg^{2+} (> 1 M).

Figs. 9 *B* and 11 compare the effects of vacuolar K^+, Rb^+, NH_4^+, and Na^+ on Ca^{2+} binding. K_{I4} increases with increasing vacuolar [K^+] reflecting the associated increasing occupancy of a vacuolar monovalent cation site (site 7). There was no detectable voltage dependence observed for this effect, and the range of values for δ_7 (electrical distance of site 7 from the vacuolar side) that is consistent with the data is $\delta_7 < 0.2$.

Therefore the data in Fig. 12 were fitted with Eq. 13, where it is assumed that $\delta_7 = 0$:

$$K_{I4}(a_K) = K_{I4}(0) + K_{I4}(\infty)\cdot(1 + K_{D7}/a_K)^{-1} \quad (13)$$

The parameter values derived from the fit are $K_{I4}(\infty) = (3 \pm 2)$ M, $K_{I4}(0) = 73$ mM, and $K_{D7} = (30 \pm 25)$ mM. The relative effects of other cations on the magnitude of K_{I4} shown in Fig. 11 are as follows: K^+ (1) > Rb^+ (0.15) > NH_4^+ (0.056) > Na^+ (<0.02).

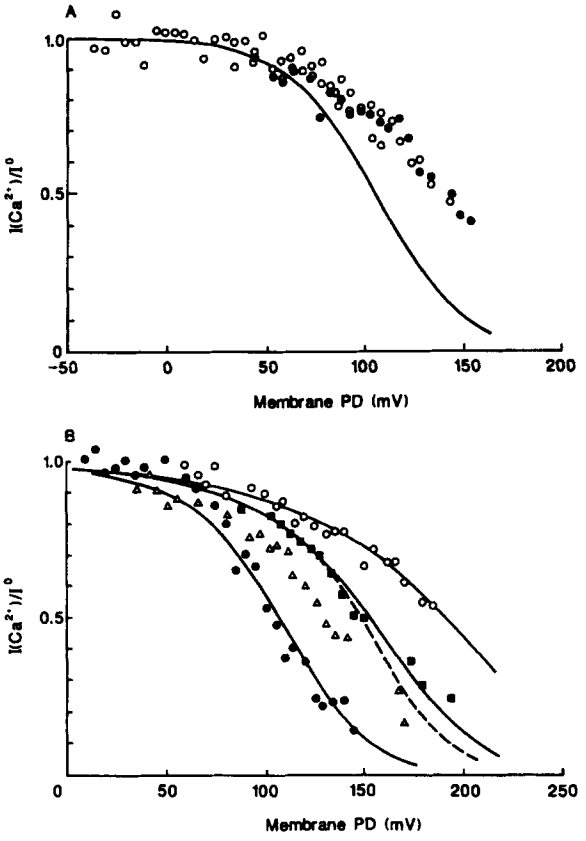

FIGURE 9. The effects of vacuolar cations on the rapid Ca^{2+} blocking kinetics from the cytoplasmic side. Cytoplasmic $[Ca^{2+}]$ = 1 mM and cytoplasmic [KCl] = 150 mM. The cytoplasmic $[Ca^{2+}]$ present for the control measurements was in the range 10–100 μM. The range of values for the ion activity coefficients in the analysis are $\tau_{K^+} = 0.7$–0.71 and $\tau_{Ca^{2+}} = 0.24$–0.26. (*A*) The ion concentrations in the vacuolar solutions are 3 mM KCl (●), 3 mM KCl + 147 mM NaCl (○), and 150 mM NaCl (*line*). The line is a fit of Eq. 11 to the data taken from *B*. (*B*) The ion concentrations in the vacuolar solutions are 150 mM KCl (○), 10 mM KCl + 140 mM NaCl (■), 10 mM RbCl+ 140 mM NaCl (△), and 150 mM NaCl (●). The Ca^{2+} block in the presence of vacuolar 150 mM NH_4Cl (data not shown) was approximately the same as that in the presence of 10 mM KCl. The curves show the least-squares fits of the data to Eq. 11 (*solid lines*, competitive binding) and Eq. 12 (*dashed lines*, noncompetitive binding). The parameters of the fit with Eq. 11 are: $K_{I3}(0) = (11.8 \pm 0.4)$ mM, $\delta_3 = -0.21 \pm 0.02$, and $\delta_4 = -0.6 \pm 0.05$. The values for $K_{I4}(0)$ are shown in Fig. 10.

To detect a noninhibited component of the current, experiments were performed under conditions where divalent ion sites were expected to be nearly saturated. For example, at membrane PDs >200 mV cytoplasmic 1 mM Ca^{2+} in the absence of vacuolar K^+ occupies site 4 >99% of the time. Under these conditions Ca^{2+} was also found to totally inhibit the current (data not shown). Hence it can be said that Ca^{2+} at site 4 totally blocks conduction. However, it is difficult to discern whether Ca^{2+} at site

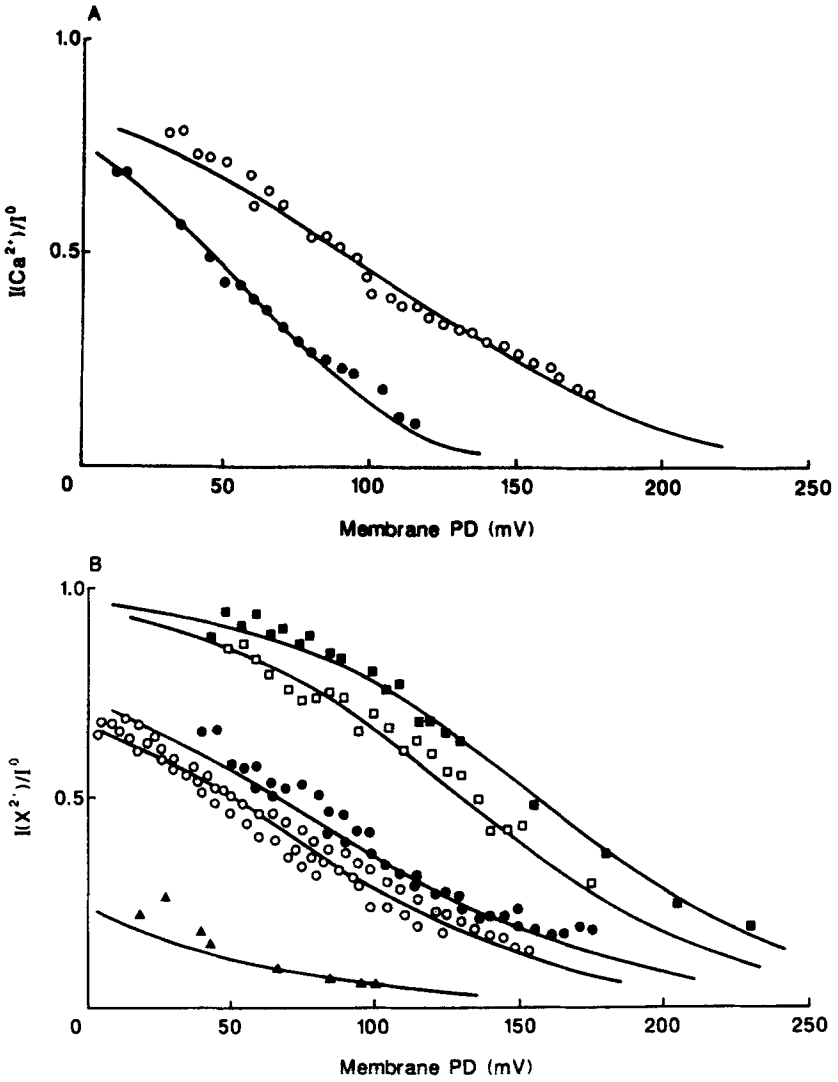

FIGURE 10. The effects of vacuolar cations on the cytoplasmic block by several divalent ions when cytoplasmic [KCl] = 150 mM. The solid lines are fits to the data with Eq. 11. (*A*) Block by 10 mM Ca^{2+} when the vacuolar solution contains 150 mM KCl (○) and 150 mM NaCl (●). When vacuolar K^+ is removed the voltage dependence of the Ca^{2+} block is increased. (*B*) Block by 1 mM $Pt(NH_3)_4^{2+}$ (*squares*), 10 mM Mg^{2+} (*circles*), and 100 mM Mg^{2+} (*triangles*) in the presence of either vacuolar 150 mM KCl (*filled symbols*) or 150 mM NaCl (*open symbols*). The voltage dependence of the block by $Pt(NH_3)_4^{2+}$ and Mg^{2+} is not affected by vacuolar [K^+]. The range of values for the ion activity coefficients in the analysis are τ_{K^+} = 0.62–0.71 and $\tau_{X^{2+}}$ = 0.14–0.26. The parameters of the fits are δ for Mg^{2+} and Ca^{2+}: $\delta_3 = -0.21 \pm 0.02$ and $\delta_4 = -0.6 \pm 0.05$; δ for $Pt(NH_3)_4^{2+}$: $\delta_3 = -0.29 \pm 0.02$. $K_{I3}(0)$ in the presence and absence of vacuolar 150 mM K^+ and K_{I4} in the absence of vacuolar K^+, respectively. Ca^{2+}: $K_{I3}(0)$ = (11.8 ± 0.4) mM, (8 ± 2) mM; $K_{I4}(0)$ = (7 ± 5) M. Mg^{2+}: $K_{I3}(0)$ = (8 ± 1) mM, (6 ± 1) mM; $K_{I4}(0) > 1$ M. $Pt(NH_3)_4^{2+}$: $K_{I3}(0)$ = (9 ± 1) mM, (5.2 ± 0.5) mM; $K_{I4}(0) > 1$ M.

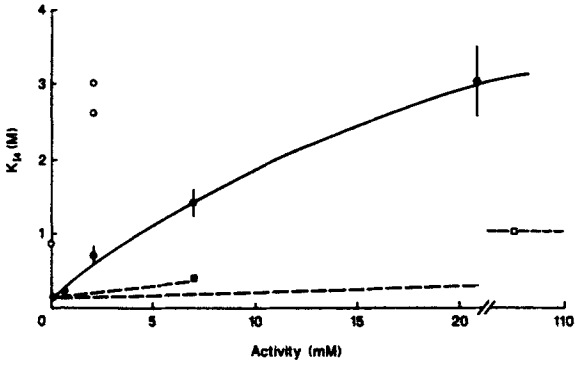

FIGURE 11. The effect of vacuolar cation activity on K_{14}; i.e., the binding of Ca^{2+} at site 4. The data are (symbol, cytoplasmic $[K^+]$ (millimolar), external cation, X^+): (●) 150, K^+; (○), 500, K^+; (■) 150, Rb^+; (□) 150, NH_4^+. Where possible, the ionic strengths of the external solutions were made up to 150 mM with NaCl. The solid curve is a fit to the K^+ data with Eq. 13. The parameters of the fit are: $K_{14}(\infty)$ = (3 ± 2) M, $K_{14}(0)$ = 73 mM, and K_{D7} = (30 ± 25) mM.

3 can also totally inhibit the current because at extreme membrane PD Ca^{2+} binding at site 4 becomes significant even in the presence of high vacuolar $[K^+]$. Block at site 3 is better studied using Mg^{2+}, which does not bind appreciably with site 4. Fig. 10 shows that 110 mM Mg^{2+} at a membrane PD of 100 mV blocks 95% of the current. This fits well with the predictions of Eq. 11, where it is assumed that divalent ion

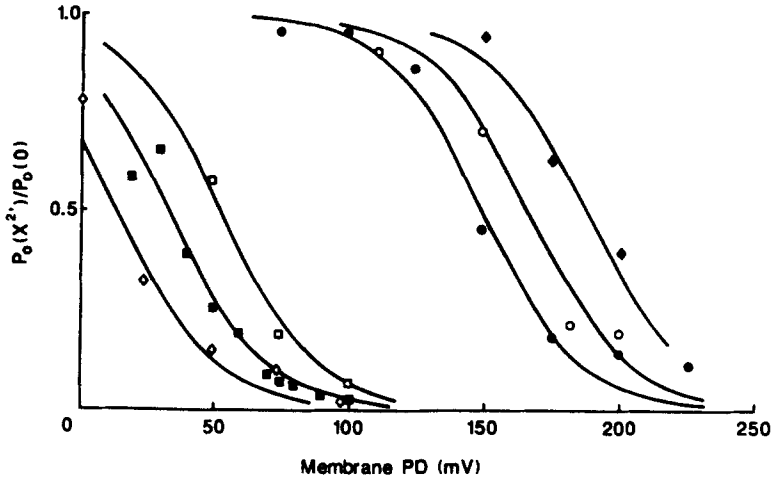

FIGURE 12. The slow cytoplasmic block of the channel shown by the relative open probability of the channel. The relative open probability is the ratio of the open probability of the blocked channel to that of the channel at low divalent ion concentrations. The data show divalent cation block and the solid lines are fits of the data to Eq. 11. The composition of bathing solutions (external, cytoplasmic, millimolar) and the fitted values of $K_{15}(0)$ associated with each are: (□) 150 NaCl, 150 KCl + 1 $CaCl_2$, (6.3 ± 1) mM; (◇) 150 NaCl, 150 KCl + 10 $CaCl_2$, (6.3 ± 1) mM; (■) 150 NaCl, 500 KCl + 10 $CaCl_2$, (8.3 ± 2) mM; (○) 150 KCl, 150 KCl + 1 $CaCl_2$, (3.0 ± 1) M; (●) 150 KCl, 500 KCl + 10 $CaCl_2$, (5.7 ± 1) M; (◆) 150 KCl, 150 KCl + 0.1 $CaCl_2$ + 1 $Pt(NH_3)_4(ClO_4)_2$, > 20 M, where $\delta_5 = -0.7 \pm 0.07$.

binding totally blocks the current. Therefore it appears that, at least in the case of Mg^{2+}, binding at site 3 causes a complete block of the pore.

Slow Block from the Cytoplasmic Side

Divalent cations block the channel from the cytoplasmic side, producing long closures. During these intervals the current through the channel drops to zero,

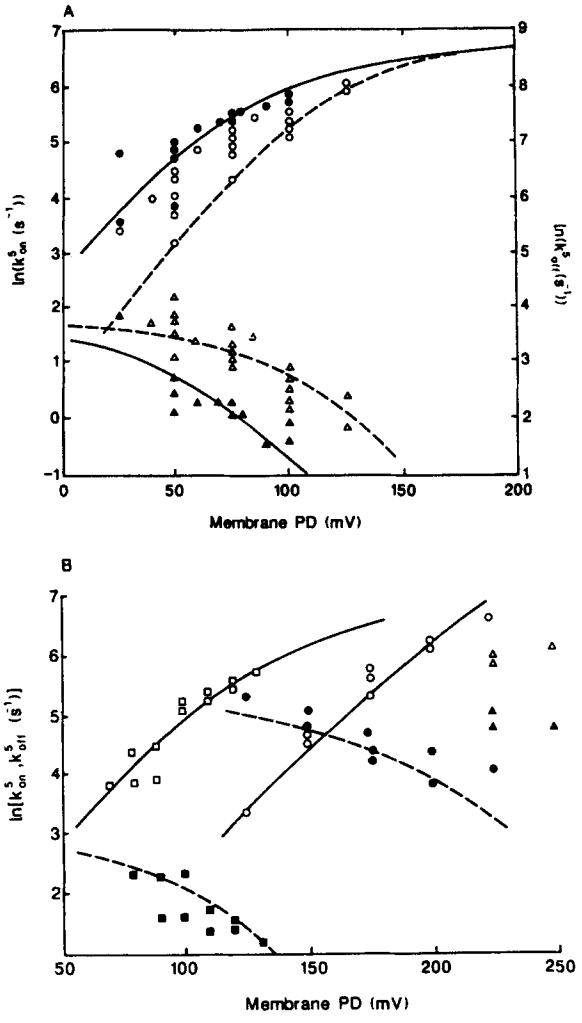

FIGURE 13. The Ca^{2+} dissociation, k^5_{off}, and association rates, k^5_{on}, derived from the channel burst and gap durations in the presence of cytoplasmic Ca^{2+} (see Materials and Methods). (*A*) k^5_{on} (*circles*) and k^5_{off} (*triangles*) in the presence of external 150 mM NaCl and cytoplasmic 150 mM KCl. Cytoplasmic $[Ca^{2+}]$ is either 1 mM (*open symbols*) or 10 mM (*filled symbols*). The lines are predictions of a sequential binding model (Eqs. 16 [*solid*] and 17 [*dashed*]) for Ca^{2+} (Scheme 1) when cytoplasmic $[Ca^{2+}]$ is either 1 mM (*dashed*) or 10 mM (*solid*). The parameters of the fit are: $(\delta_5 - \delta_4) = -0.1$, $k_{45}(0) = 200\ s^{-1}$, $k_{54}(0) = 40\ s^{-1}$. (*B*) k^5_{on} (*open symbols*) and k^5_{off} (*filled symbols*) in the presence of cytoplasmic 500 mM KCl and 10 mM $CaCl_2$. External solution contains: 150 KCl (●); 150 NaCl (■); and 500 mM KCl (▲). The parameters of the fit are: $(\delta_5 - \delta_4) = -0.1$; $k_{45}(0) = 200\ s^{-1}$, $k_{54}(0) = 60\ s^{-1}$ in zero external $[K^+]$; $k_{45}(0) = 30\ s^{-1}$, $k_{54}(0) = 7{,}000\ s^{-1}$ in 150 mM external $[K^+]$ (this parameter value is not significant due to the uncertainty in the parameter value of P_4).

indicating a total block of the channel. The time average of the resulting block by Ca^{2+} and $Pt(NH_3)_4^{2+}$ is shown in Fig. 12 by the open probability of the channel which is fitted with Eq. 14:

$$P_o(X^{2+})/P_o(0) = (1 + a_X/K_{I5})^{-1} \qquad (14)$$

where K_{I5} has a voltage dependence similar to that given by Eq. 6. The voltage

dependence of the block indicates a binding site deep within the pore ($\delta_5 = -0.7 \pm 0.07$) which is the same as that found previously for block by Ca^{2+} and also Ba^{2+} and Sr^{2+} (Laver and Walker, 1991). $K_{I5}(0)$ depends on $[K^+]$ in both the cytoplasmic and vacuolar solutions. In the absence of vacuolar K^+, increasing cytoplasmic $[K^+]$ from 150 to 500 mM increases $K_{I5}(0)$ for Ca^{2+} from 6.3 ± 1 mM to 8.3 ± 2 mM. Exchanging vacuolar 150 mM Na^+ for K^+ increases $K_{I5}(0)$ for Ca^{2+} by a factor of 600. Combining data presented here with those in Laver and Walker (1991), the binding selectivity of site 5 for divalent ions ($K_{I5}(0)$ in 150 mM symmetric K^+) is: Ba^{2+} (1.2 mM) > Sr^{2+} (47 mM) > Ca^{2+} (10 M) > Mg^{2+} (>47 M), and $Pt(NH_3)_4^{2+}$ (>20 M).

Ca^{2+}-induced channel closures occur with durations that follow an exponential frequency distribution. The frequency distributions of burst lengths can also described by a single exponential. Hence the voltage dependence of Ca^{2+} binding rates at site 5 (k^5_{off} and k^5_{on}) shown in Fig. 13 could be derived from the mean burst and gap durations (see Materials and Methods). These results were usually obtained from patches with one channel, though under conditions of low channel activity patches with two channels were also suitable. The number of channels in each patch could be determined from the number of different current levels observed under conditions of high channel open probability (i.e., at membrane PDs where ion block is not significant).

k^5_{off} exhibits an *e*-fold change every 60–80 mV (Fig. 13 *A* and *B*). The voltage dependence of k^5_{on} starts to plateau under conditions where sites 3 and 4 become saturated with Ca^{2+}, which is an indication of competition between sites 3, 4, and 5 for Ca^{2+}.

The $[Ca^{2+}]$ dependence of k^5_{on} and k^5_{off} under conditions where sites 3 and 4 approach saturation yields further information about competitive interactions between these sites. Such conditions occur within the experimental voltage range when the cytoplasmic solution contains 150 mM KCl and the vacuolar solution contains 150 mM NaCl. Here increasing cytoplasmic $[Ca^{2+}]$ from 1 to 10 mM decreased k^5_{off} approximately fivefold and increased k^5_{on} approximately twofold (see Fig. 13 *A*).

Fig. 13 *B* shows how vacuolar K^+ reduces internal Ca^{2+} block by both increasing k^5_{off} and decreasing k^5_{on}. Analysis of k^5_{on} and k^5_{off} in terms of reaction rate is carried out within the framework of a model for Ca^{2+} binding which is justified in the Discussion. Hence analysis of the $[K^+]$ dependence of these reaction rates is reserved for the Discussion.

DISCUSSION

The results were fitted with a model that proposed five divalent ion binding sites on the K^+ channel protein (see Fig. 15). Two of the sites are accessible to ions in the vacuolar solution (sites 1 and 2) and three to ions in the cytoplasmic solution (sites 3–5). The observed blocking characteristics associated with the binding of Ca^{2+} with these sites are described in the next section and are also summarized in Table I.

The model also proposed two sites for monovalent cations on the protein. Site 7 is located superficially ($\delta_7 < 0.2$) at the vacuolar end of the channel and site 6 is a deeper site ($\delta_6 = -0.3 \pm 0.1$) at the cytoplasmic end of the pore.

The properties of these sites are interpreted in terms of the conventional view of maxi-K channel protein structure (e.g., Latorre and Miller, 1983; Eisenman and Dani, 1987); the pore consists of a short constricted section which opens out into vestibules that face the bulk solutions on each side of the membrane.

Ca^{2+} Sites

Vacuolar sites. Site 1 is a relatively superficial site ($\delta_1 = 0.07$) which is assumed to be responsible for the Ca^{2+}-induced inhibition of K^+ conductance.

Site 2 is located deeper within the pore ($\delta_2 = 0.3$) which is assumed to be responsible for the slow block by vacuolar Ca^{2+}. The ion binding events at this site are slow enough (0.1–1 ms) to be easily resolved by the patch-clamp technique. Ca^{2+} binding at this site has been shown to be coupled with the operation of one of the voltage-dependent gates of the channel (Laver, 1990). Site 2 is occluded from the vacuolar solution when the gate is closed, and when Ca^{2+} does bind and block the channel it also locks the gate in the open conformation.

At physiological ionic strength the voltage dependences of Ca^{2+} dissociation and association rates (Fig. 5) are consistent with Ca^{2+} dissociating from site 2 mainly by returning either to the vacuolar solution or possibly to site 1. However, under low ionic strength conditions when Ca^{2+} dwells at site 2 for longer periods the voltage dependence of the dissociation rate indicates the additional dissociation route for Ca^{2+} to the cytoplasmic solution. In this way Neyton and Miller (1988*a*) also showed that Ba^{2+} could permeate the maxi-K channel in rat skeletal muscle. The lower values of k^2_{off} obtained in cytoplasmic solutions of low ionic strength may be due to the effect of negative fixed charge on the cytoplasmic side of the channel (Laver, D. R., and K. A. Fairley, unpublished data) which would shift the voltage dependence of channel kinetics to more positive membrane PDs. These effects have already been observed with the maxi-K channel from rat (MacKinnon, Latorre, and Miller, 1989). Regardless of the exact mechanism for the effect of ionic strength on the dissociation rate it appears that these conditions allow the effects of Ca^{2+} permeation in the channel, which would otherwise occur well outside the experimental range, to be measured. The dissociation rate of Ca^{2+} to the cytoplasmic solution is weakly voltage dependent and is in the range 10^2–10^3 s^{-1}. The permeation rate of vacuolar Ca^{2+} in the channel is the product of the occupancy of site 2 (see Fig. 4) and the dissociation rate. The Ca^{2+} permeation rate so calculated varies from 5 s^{-1} at 0 mV to 500 s^{-1} at −200 mV.

Cytoplasmic sites. Sites 3 and 4 are located at 21 and 60% of the way along the membrane PD (from the cytoplasmic side), respectively. These sites that are responsible for cytoplasmic Ca^{2+} inhibition of channel conductance are assumed to exhibit rapid binding kinetics.

Site 5 is located deep within the pore ($\delta_5 = -0.7$) and the Ca^{2+} binding kinetics at this site are slow. The ion association and dissociation rates have opposite voltage dependences of similar magnitude, which suggests that Ca^{2+} at this site dissociates primarily back to the cytoplasmic side.

Sites 2 and 5 appear to be located on the same membrane plane within the pore, which raises the possibility that they are in fact the same site. However, this cannot be the case because sites 2 and 5 have quite different properties. For example, Ca^{2+} at site 2 exits rapidly to the vacuolar solution with a dissociation rate of 5.4×10^4 s^{-1} at

50 mV. At this membrane PD Ca^{2+} at site 5 has a low dissociation rate which ranges from 20 to 150 s^{-1}, where most of these dissociation events involve Ca^{2+} exiting to the cytoplasmic solution rather than the vacuolar solution.

Competition between Divalent Ion Sites

The concentration dependence of the Ca^{2+} block over a wide range fits well with that expected from Ca^{2+} binding to discrete saturable sites on the channel protein (Fig. 8). The two rapid cytoplasmic sites appear to compete for Ca^{2+}. The voltage dependence of the rapid Ca^{2+} block in Fig. 9 *B* fitted better with the predictions of a competitive kinetic model than with a model where it was assumed that Ca^{2+} binds independently at sites 3 and 4.

Competition between rapid and slow sites for Ca^{2+} can be determined from the $[Ca^{2+}]$ dependence of the Ca^{2+} association and dissociation rates. If Ca^{2+} only binds to a site when the other divalent ion sites in the same vestibule are unoccupied, then the association rates at sites 2 and 5 have the following concentration dependence:

$$k_{on}^{(i)}(a_{Ca}) = a_{Ca}k^{o(i)}(1 - P); \qquad i = 2 \text{ or } 5 \tag{15}$$

where a_{Ca} is the Ca^{2+} activity, $k^{o(i)}$ is the association rate constant for an unoccupied channel, and P is the probability that other sites in the same vestibule are occupied. In Eq. 15 $k_{on}^{(i)}$ is proportional to a_{Ca} at low concentrations and levels off at high concentrations where P approaches one. It is also possible that Ca^{2+} at sites 2 or 5 can be "locked in" to the channel by Ca^{2+} at a more superficial site (Neyton and Miller, 1988*b*). In that case $k_{off}^{(i)}$ will decrease as the other sites in the same vestibule saturate due to either high $[Ca^{2+}]$ or membrane PD. Laver (1990) found that k_{on}^{2} does saturate at high vacuolar $[Ca^{2+}]$ and that k_{off}^{2} is independent of vacuolar $[Ca^{2+}]$. In this way it was established that sites 1 and 2 cannot be simultaneously occupied.

However, the same conclusion cannot be drawn from the blocking kinetics of cytoplasmic Ca^{2+}. The dissociation rate from site 5 is found to decrease with increasing occupancy of sites 3 and 4. Hence two Ca^{2+} can occupy the vestibule that faces the cytoplasmic side; one at site 5 and another at either site 3 or 4, which locks Ca^{2+} into site 5. The Ca^{2+} association rate saturates at high cytoplasmic $[Ca^{2+}]$, which means that Ca^{2+} cannot bind at site 5 when sites 3 or 4 are occupied. This does not imply sites 3–5 compete for Ca^{2+} because it has just been shown that two Ca^{2+} can occupy the cytoplasmic vestibule. Rather, this means that Ca^{2+} at the superficial sites occludes the deep site. These properties are characteristic of a kinetic scheme where the cytoplasmic solution (state 0) and sites 3–5 are connected in series. The "lock in" effect contributes an additional state where Ca^{2+} is bound at site 5 and site 3 or 4.

$$0 \leftrightarrow (3 \leftrightarrow 4) \leftrightarrow (5 \leftrightarrow [\text{lock in}])$$

Rapid block Slow block

Scheme 1

For such a model the association and dissociation rates are given by Eqs. 16 and 17:

$$k_{on}^{5}(V) = P_4(V)k_{45}(0) \exp\left[-(\delta_5 - \delta_4)zFV/2RT\right] \tag{16}$$

$$k_{off}^{5}(V) = [1 - P_3(V) - P_4(V)]k_{54}(0) \exp\left[(\delta_5 - \delta_4)zFV/2RT\right] \tag{17}$$

where $k_{54}(0)$ and $k_{45}(0)$ are the rate constants for Ca^{2+} exchange between sites 4 and 5 at zero voltage. P_3 and P_4 are the voltage-dependent probabilities that sites 3 and 4 are occupied while site 5 is occupied. The occupancies of sites 3 and 4 are likely to depend on whether site 5 is occupied. However, here it is assumed that the values for P_3 and P_4 are independent of the occupancy of site 5 so that the values in Eq. 17 can be obtained from the analysis of the rapid Ca^{2+} block where site 5 is empty. The solutions of Eqs. 16 and 17 predict the gross features of the $[Ca^{2+}]$ and voltage dependences of k^5_{off} and k^5_{on} shown in Fig. 12, *A* and *B*. The exponential term in Eq. 17, where $(\delta_5 - \delta_4) = -0.1$, accounts for only 15–25% of the observed voltage dependence of k^5_{off}. The rest of the voltage dependence comes from the voltage dependence of the lock in effect.

Competition between Divalent and Monovalent Cations

The vestibule facing the vacuole. All forms of vacuolar and cytoplasmic Ca^{2+} block were alleviated by an increase in $[K^+]$ on the same side of the channel. This indicates that there is a limit to the number of ions that can occupy each vestibule so that the K^+ and Ca^{2+} sites compete for ions.

In a previous study of the properties of Ca^{2+} binding at site 1 in the presence of high $[K^+]$ (Laver, 1990) it was found that Ca^{2+} block was predicted by single-ion models; i.e., only one ion could occupy the channel at any one time. However, single-ion models fall short of explaining the Ca^{2+} inhibition of conductance at low vacuolar $[K^+]$ in Fig. 3. The biphasic inhibition is a characteristic of both multi-ion occupancy of the pore and surface charge effects. To illustrate how this arises from multi-ion kinetics, consider the following scheme for rapid ion binding in the vacuolar vestibule. It can be empty (state 0), occupied by either one K^+ (state K) or Ca^{2+} at site 1 (state Ca), occupied by both K^+ and Ca^{2+} together (state KCa), or occupied by two K^+ (state 2K).

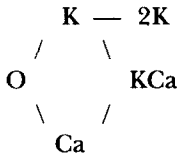

Scheme 2

Ions binding to channels that already contain one ion are expected to do so with relatively low affinity due to the effects of ion repulsion. It serves the purpose of this illustration to make the simplifying assumption that ions are in equilibrium with the vacuolar solution and that the K^+ current associated with each state, I_{state}, is proportional to the mean K^+ occupancy, P_{state}, of that state:

$$I = I_K \cdot P_K + I_{KCa} \cdot P_{KCa} + I_{2K} \cdot P_{2K} \tag{18}$$

The occupation probabilities for the states are related to the dissociation constants in the kinetic scheme. Hence:

$$I = \frac{I_K \cdot a_K / K_{DK} + I_{KCa} \cdot a_K a_{Ca} / K_{DK} K_{DKCa} + I_{2K} \cdot a_{K^2} / K_{DK} K_{D2K}}{1 + a_K / K_{DK} + a_K a_{Ca} / K_{DK} K_{DKCa} + a_{K^2} / K_{DK} K L_{D2K} + a_{Ca} / K_{DCa}} \tag{19}$$

Here a_K and a_{Ca} are the vacuolar K^+ and Ca^{2+} activities, respectively. K_{DK} and K_{D2K} are the dissociation constants for the first and second K^+, K_{DCa} is that for Ca^{2+}, and K_{DKCa} is that for K^+ in the presence of bound Ca^{2+}.

The solution to this equation is compared with the data in Fig. 3. At low $[K^+]$ and $[Ca^{2+}]$ only states 0, Ca, and KCa have significant probabilities. Ion binding under these conditions will reflect competition between these high affinity sites. The noninhibited component of the current which is observable when $[Ca^{2+}]$ is high and $[K^+]$ is low arises from K^+ permeation through the channel in the presence of bound Ca^{2+}; i.e., state KCa is a conducting state (I_{KCa} is nonzero). In the limit of high $[K^+]$ only states K, KCa, and 2K have significant probabilities, and when $I_{2K} \gg I_K$ Eqs. 18 and 19 reduce to a form that is the same as that used for predicting ion block of single-ion channels. This explains the success of single-ion models in accounting for the Ca^{2+} block in previous studies. Hence, contrary to the previous conclusion drawn by Laver (1990) at least one K^+ and one Ca^{2+} can simultaneously occupy the vacuolar vestibule of the channel.

The alternative explanation is that Ca^{2+} can not only bind but can also screen fixed charges on the channel or the membrane (Moczydlowski, Alvarez, Vergara, and Latorre, 1985; MacKinnon et al., 1989; Villarroel and Eisenman, 1989). A surface charge density as small as -5×10^{-4} C/m^2 in the vacuolar vestibule in conjunction with single-ion binding kinetics could account for the Ca^{2+} block. The most convincing evidence against this alternative is found in Fig. 9*A*, which shows that cytoplasmic Ca^{2+} block is independent of the ionic strength of the vacuolar solution. Gouy-Chapman theory predicts that a surface charge of -5×10^{-4} C/m^2 will generate a surface potential of -43 mV in a solution with an ionic strength of 3 mM and -8 mV in 150 mM. This surface potential offsets the trans-pore PD from the membrane PD. Such an increase in ionic strength would shift the Ca^{2+} block as shown in Fig. 9*A* by 35 mV to the right along the voltage axis. Even though cytoplasmic Ca^{2+} block was found to be very sensitive to vacuolar $[K^+]$, it was independent of vacuolar ionic strength.

The competitive binding of K^+ and Ca^{2+} at site 2 has also been reported by Laver (1990). It is difficult to determine whether a competitive mechanism similar to site 1 applies to site 2. This is because it is not possible to obtain reliable measurements of open and closed durations of channels when the unitary currents are small, such as is the case when modeling Ca^{2+} binding at site 1. However, one obvious difference in the K^+-Ca^{2+} competition at sites 1 and 2 is that Ca^{2+} at site 2 can totally block the current, whereas Ca^{2+} at site 1 allows K^+ permeation.

The vestibule facing the cytoplasm. Rapid binding of cytoplasmic Ca^{2+} is alleviated by cytoplasmic K^+ and single-ion models cannot account for the observed results. First, these models predict that an increase in $[K^+]$ from 150 to 500 mM (a 2.8-fold increase in activity) cannot increase the observed K_I for the Ca^{2+} block by a factor greater than 2.8. Second, they predict that K^+ will alter Ca^{2+} binding at all the cytoplasmic sites in the same proportion. However, cytoplasmic K^+ is shown here to increase K_{I3} and K_{I5} by a factor of 1.9 and K_{I4} by a factor of 4.3.

To illustrate how multi-ion kinetic models can predict these competitive effects, consider kinetic Scheme 3. Scheme 3 is similar to that used for describing the ion binding kinetics at the vacuolar vestibule except that in this case two cytoplasmic

Ca^{2+} sites are included.

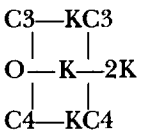

Scheme 3

The states and dissociation constants are named according to the convention used for Scheme 2. States C3 and C4 refer to Ca^{2+} bound at sites 3 and 4, respectively. In a similar way to the derivation of Eq. 19 it can be shown that the probabilities of states C3, C4, KC3, and KC4 occurring are given by Eqs. 20–22:

$$P_{C(i)} = Aa_{Ca}/K_{DC(i)}; \qquad i = 3 \text{ or } 4 \tag{20}$$

and

$$P_{KC(i)} = Aa_K a_{Ca}/K_{DK}K_{DC(i)}; \qquad i = 3 \text{ or } 4 \tag{21}$$

and where

$$A = \left\{1 + \frac{a_{K^2}}{K_{DK}K_{D2K}} + \frac{a_K}{K_{DK}} + \frac{a_{Ca}}{K_{DC3}} + \frac{a_{Ca}}{K_{DC4}} + \frac{a_K a_{Ca}}{K_{DK}K_{DC3}} + \frac{a_K a_{Ca}}{K_{DK}K_{DC4}}\right\}^{-1} \tag{22}$$

where a_K and a_{Ca} are the cytoplasmic K^+ and Ca^{2+} activities.

The results show that Ca^{2+}, when bound to sites 4 and 5 and also possibly site 3, totally blocks the K^+ current. Hence in Scheme 3 the only conducting states are K and 2K. States KC4 and probably KC3 do not contribute to the total current; i.e., Ca^{2+} is assumed to totally block the channel from the cytoplasmic side. To explain the strong competition between K^+ and Ca^{2+}, consider the case when Ca^{2+} and K^+ are unable to simultaneously occupy the pore; i.e., states KC3 and KC4 have low probabilities. Rearranging Eqs. 20–22 then reveals that the half-inhibition constants associated with sites 3 and 4 have the following dependence on a_K:

$$K_{I(i)} = K_{DC(i)}(1 + a_K/K_{DK} + a_{K^2}/K_{DK}K_{D2K}); \qquad i = 3 \text{ or } 4 \tag{23}$$

Thus increasing a_K by a factor of 2.8 could increase K_{I3} and K_{I4} as much as 8.3-fold, i.e., proportional to a_K^2.

To address the problem of why K^+ competes differently with Ca^{2+} at sites 3 and 4, consider the case when states KC3 and KC4 have high probabilities of occurrence. Then K_{I3} and K_{I4} can be shown to be approximately proportional to a_K rather than a_K^2:

$$K_{I(i)} = K_{DC(i)}(K_{DK}/a_K + 1 + a_K/K_{D2K}); \qquad i = 3 \text{ or } 4 \tag{24}$$

If KC3 has a high probability and KC4 has a low probability of occurrence, then cytoplasmic $[K^+]$ could have a much stronger effect on Ca^{2+} binding at site 4 than at site 3. The fact that this is observed suggests that one Ca^{2+} at site 3 can occupy the pore along with one K^+, while Ca^{2+} at site 4 almost completely excludes K^+ from the pore. In a similar way it can be argued that Ca^{2+} can occupy site 5 while one K^+ is in the pore.

Trans-Channel Competition

The slow blocking kinetics of cytoplasmic Ca^{2+} has been analyzed in terms of a sequential binding model (Scheme 1). The effect of vacuolar K^+ is analyzed here by its effect on the model parameters. Increasing vacuolar K^+ is interpreted as an increase in the dissociation rate constant (see Eq. 17). Fig. 14 shows the sublinear $[K^+]$ dependence of k_{54} (0 mV) which is fitted with Eq. 25:

$$k_{54}(a_K) = k_{54}(0) + k_{54}(\infty) \cdot (1 + K_{D7}/a_K)^{-1} \quad (25)$$

where a_K is the vacuolar K^+ activity and K_{D7} is the K^+ dissociation constant at site 7. The kinetics of the rapid cytoplasmic Ca^{2+} block shows that δ_7 is so small that in Eq.

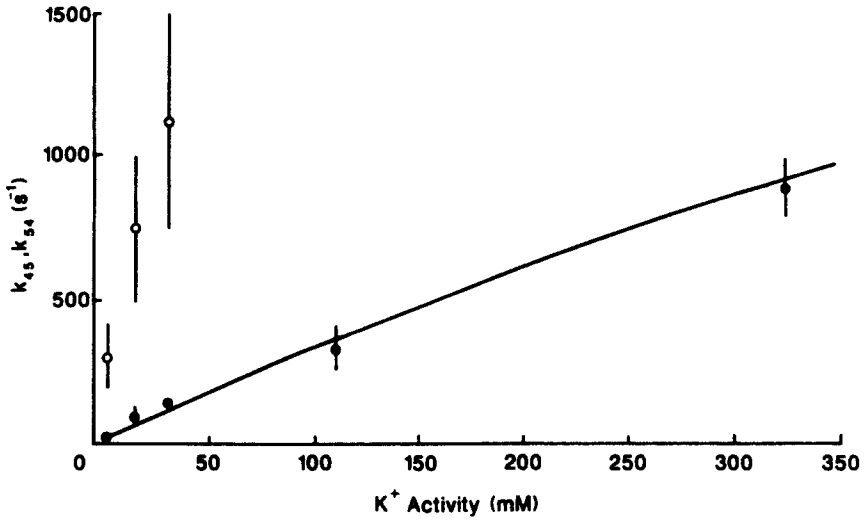

FIGURE 14. The external $[K^+]$ (a_K) dependence of the Ca^{2+} binding rate constants at zero membrane PD, k_{54} (*filled symbols*) and k_{45} (*open symbols*). The curve represents the fit of Eq. 25 with the data. The parameters of the fit are: $k_{45}(a_K = 0) = 20\ s^{-1}$, $k_{45}(a_K = \infty) = (5{,}500 \pm 4{,}000)\ s^{-1}$, $K_{D7} = (1.7 \pm 1)$ M. The large errors on k_{54} data are primarily due to uncertainties in estimates of the occupancy of site 4, P_4.

25 it is assumed to be zero. Site 7 has a relatively low affinity compared with site 6 ($K_{D7} > 500$ mM).

Within the framework of Scheme 1, the vacuolar K^+-induced decrease in k^5_{on} is due to an associated decrease in the occupancy of site 4. Furthermore, vacuolar $[K^+]$ has a small but opposite effect on the association rate constant k_{45} which increases with increasing vacuolar $[K^+]$ (see Fig. 14). It therefore appears that vacuolar K^+ raises the energy of the minima associated with the cytoplasmic Ca^{2+} sites but does not have as strong an effect on the energy barriers between the sites.

Binding of Ca^{2+} to the two outer-most sites on each side of the channel is weakly dependent on $[K^+]$ on the opposite side of the pore, whereas the deeper sites (sites 2, 4, and 5) are strongly affected by K^+. The fact that Ca^{2+} at site 1 does not interact

with K^+ in the opposite vestibule is not surprising since it has been shown that K^+ and Ca^{2+} can also cohabit in the vacuolar vestibule (see previous section).

Analysis of the slow blocking kinetics at sites 2 and 5 shows that K^+ increases the Ca^{2+} dissociation rates. For this to occur both Ca^{2+} and K^+ must simultaneously occupy opposite ends of the pore. The fact that trans-channel competition is more pronounced for the deep Ca^{2+} sites is consistent with them being in closer proximity to the monovalent cation sites in the opposite vestibule.

One explanation for why $[K^+]$ has different effects on k_{on} and k_{off} for Ca^{2+} binding in the opposite vestibule has been provided by Neyton and Miller (1988*b*). They point out that k_{off} is measured while the channel is blocked and in equilibrium. Hence the saturating $[K^+]$ dependence of k_{off} can be used to measure the occupancy of the K^+ site. However, k_{on} is measured when the channel is conducting and K^+ is not in equilibrium so that saturating curves fitted with variations in k_{on} give misleading estimates of the occupancy of the K^+ site.

The different effects of $[K^+]$ on k_{on} and k_{off} also reflect other differences between the blocked and unblocked states of the pore. For example, measurements of vacuolar Ca^{2+} binding were made here at negative membrane PDs where K^+ can permeate the channel from the vacuolar side and bind to and saturate site 6 on the cytoplasmic side. Thus small changes in cytoplasmic $[K^+]$ would have little effect on the occupancy of site 6. However, when the channel is blocked by Ca^{2+} site 6 is only accessible to ions from the cytoplasmic solution, thus revealing the binding kinetics of cytoplasmic K^+.

Ion Selectivity

By considering binding between hydrated ions Eisenman (1961) showed that the equilibrium selectivity of an anionic site for monovalent cations (group Ia) could be modeled on the basis of a balance between ion–water and ion–site interactions. He concluded first that the order of ion specificity is largely determined by the anionic radius, or surface electric field strength, of the binding site. Second, the magnitude of the selectivity depends on the amount of water admitted into the vicinity of the binding site. Truesdell and Christ (1967) extended Eisenman's model to account for divalent ion selectivity by considering binding sites consisting of pairs of monovalent anions. They showed that these sites are selective for divalent ions over monovalent ions when the negative charges are separated by <0.5 nm. The order of selectivity among divalent ions is dependent on the anionic radii at the binding site.

The superficial divalent ion sites (sites 1 and 3) have a low selectivity which indicates that these sites have a high degree of hydration. The weak voltage dependence and selectivity both suggest that these sites are located so that they are relatively open to the bulk solutions in the channel vestibules. The cytoplasmic site (site 3) has a type VI selectivity sequence which corresponds to site radius of 0.06 nm (Truesdell and Christ, 1967). The large polyatomic divalent cation $Pt(NH_4)_3^{2+}$ binds to these sites with higher affinity than the group IIa cations. This further supports the notion that sites 1 and 3 are located on relatively accessible parts of the protein structure.

The deeper sites (sites 2, 4, and 5) have strong selectivities. For example, the selectivity of site 5 is 10^4-fold larger than that for site 3. This indicates that these deep

sites do not admit water as easily as the shallow sites. This is consistent with these sites being located in a constricted part of the pore where the ions must sacrifice their hydration shell to gain access to the binding sites. These sites have a selectivity sequence that corresponds to type VII which is expected from a site with anionic radii >0.07 nm.

The anhydrous diameter of $Pt(NH_4)_3^{2+}$ (0.7 nm) is similar to the hydrated diameters of the group IIa cations. However, unlike the water surrounding group IIa cations the amine groups are not labile. The inability of $Pt(NH_4)_3^{2+}$ to bind to the deep sites is consistent with these sites being located in a constricted part of the protein structure, possibly within the narrow part of the pore.

In this study the selectivity sequence of two monovalent cation sites has been determined. The relative ion specificities of the cytoplasmic and vacuolar sites (sites 6 and 7) are: K^+ (1, 1) > Rb^+ (0.15, 0.15) > NH_4^+ (0.06, 0.056) > Na^+ (<0.03, <0.02). Both sequences are similar to the ion permeability sequence for the channel, which is: K^+ (1) > Rb^+ (0.33) > NH_4^+ (0.11) > Na^+ (<0.06). The correlation between the ion permeability sequence and binding sequences supports the hypothesis of Neyton and Miller (1988*b*) that the permeability selectivity of the channel is associated with relatively superficial binding sites.

Location of Ion Binding Sites on the Channel Protein

The data presented here clearly show that several ions can interact simultaneously with the K^+ channel protein. Multi-ion kinetic properties of the maxi-K channel in *Chara* and in rat (Neyton and Miller, 1988*a, b*) are both interpreted as being due to ion interactions within the pore. Hence these interactions are used to probe the affinities and locations of K^+ binding sites within the pore. Draber et al. (1991) proposed an alternative permeation mechanism in the large conductance K^+ channel in *Nitella* where ion binding at channel-modifying sites outside the pore produces multi-ion kinetics. Within the framework of that model, Ca^{2+} could block K^+ permeation in the *Chara* channel by binding within a cleft in the protein structure which is not accessible to ions in the permeation pathway. Competition between K^+ and Ca^{2+} would not necessarily be due to K^+ in the pore. Hence ion interactions may reflect properties of ion binding sites outside the pore and so have no relevance to K^+ permeation.

It is difficult to distinguish between these models because it is possible to describe both processes by the same kinetic scheme. The most convincing piece of evidence for an interior location for site 2 is that Ca^{2+} can dissociate from this site to either the vacuolar or cytoplasmic side of the membrane. Circumstantial evidence for an interior location for the monovalent binding sites (sites 6 and 7) can be drawn from the fact that the ion specificities of these sites are the same as the ion permeation selectivity of the pore.

Comparison with Animal Maxi-K Channels

The maxi-K channel from rat skeletal muscle has been thoroughly characterized. The voltage dependence of site 3 is the same as that found for divalent ion binding sites on maxi-K channel in rat skeletal muscle (Oberhauser, Alvarez, and Latorre, 1988; Ferguson, 1991) and SR K^+ channel in cardiac muscle (Liu and Strauss, 1991). The

voltage dependence of Ca^{2+} binding at site 1 ($\delta_1 = 0.07$) is much less than that reported for vacuolar (trans) Ca^{2+} block of the SR channel ($\delta = 0.24$) by Liu and Strauss (1991). However, considering the low bandwidth of their measurements, a voltage-dependence "flicker block" like that observed here would not be resolved and hence would be mixed in with the rapid block and so increase the observed voltage dependence.

Ba^{2+} binds to this channel from the cytoplasmic side at a deep site ($\delta = -0.67$) (Vergara and Latorre, 1983) which corresponds to site 5 in the *Chara* K^+ channel. Detailed studies of the K^+–Ba^{2+} interactions within the rat channel were made by Neyton and Miller (1988*a*, *b*). The differences between their findings and those presented here stem mainly from the fact that Ba^{2+} can readily permeate the channel in rat at modest membrane PDs, whereas the channel in *Chara* Ca^{2+} permeation is detected only at extreme membrane PD. The channel in rat has a cytoplasmic lock in site with voltage-dependent binding kinetics ($\delta = -0.3$) that parallel those of site 6 ($\delta_6 = -0.3$). The zero voltage binding affinity of site 6 for K^+ (~ 10 mM) is much higher than that of the cytoplasmic lock in site (330 mM). This difference could be due in part to the methods used for probing these sites. Neyton and Miller (1988*b*) derived the properties of the cytoplasmic lock in site from interactions between K^+ and Ba^{2+} within the same vestibule. In the present study site 6 was probed using interactions between ions in opposite vestibules where the repulsive forces between ions are weaker. This would explain the lower observed binding affinity of the cytoplasmic lock in site compared with that for site 6. The Ca^{2+} lock in effect observed here has been previously observed in animal maxi-K channels by Neyton and Miller (1988*b*). They found that cytoplasmic Ca^{2+} could lock Ba^{2+} into the channel, indicating that Ca^{2+} and Ba^{2+} simultaneously occupy the cytoplasmic vestibule.

Evidence for a vacuolar lock in site in the rat maxi-K channel was obtained from the effect of vacuolar K^+ on Ba^{2+} permeation (Neyton and Miller, 1988*a*). Since Ca^{2+} permeation through the *Chara* channel is not easily measured, a vacuolar lock in site could not be detected by these means. The properties of site 7 do not correlate closely with any of the sites detected on the rat maxi-K channel. The location of site 7 ($\delta_7 < 0.2$) corresponds to that of the vacuolar lock in site, whereas its affinity for K^+ is more like that the vacuolar "enhancement" site.

The selectivity of the cytoplasmic divalent cation sites of the *Chara* channel are such that Mg^{2+} binds mainly to site 3 and Ba^{2+} binds mainly to site 5. Only Ca^{2+} binds appreciably to three cytoplasmic sites. Thus, studies of the blocking effects of Ba^{2+} (Neyton and Miller, 1988*a*, *b*) and Mg^{2+} (Ferguson, 1991) only reflect the characteristics of two sites, which may explain why only two cytoplasmic binding sites have been reported for the animal maxi-K channel. It is the unique properties of Ca^{2+} that have allowed the competitive interactions between the three cytoplasmic sites to be investigated here.

CONCLUSIONS

Fig. 15 presents a schematic diagram that outlines the main features of Ca^{2+} block of the large-conductance K^+ channel in *Chara*. Ca^{2+} binds to the protein at five kinetically distinct sites. The vacuolar vestibule has two Ca^{2+} binding sites (sites 1 and

2) which are located 8 and 30% of the way along the trans-pore PD from the outside, respectively. Sites 3–5 are situated in the cytoplasmic vestibule at 21, 60, and 70% along the trans-pore PD from the inside, respectively. Vacuolar Ca^{2+} has a measurable permeability in the *Chara* K^+ channel. Permeation of cytosolic Ca^{2+} was not

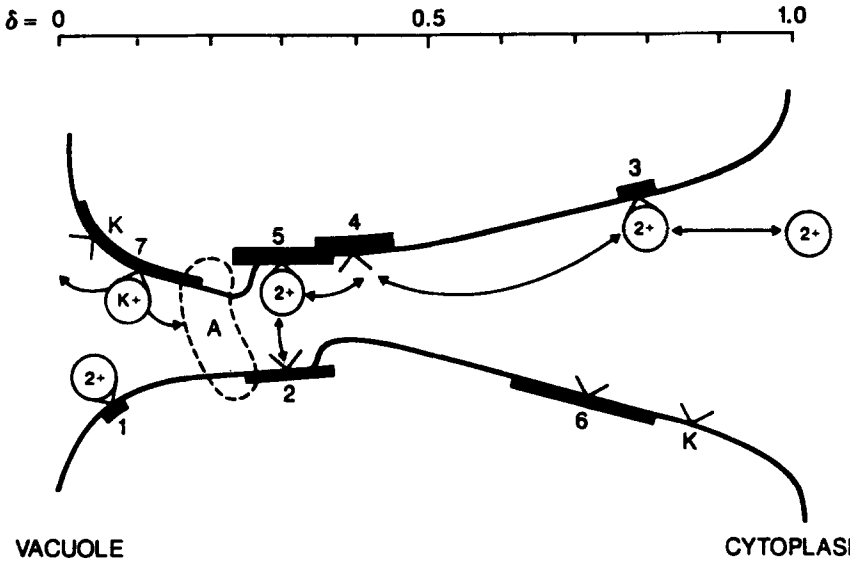

FIGURE 15. This schematic diagram summarizes the main aspects of Ca^{2+} binding with the *Chara* K^+ channel. The scale indicates the relative potential drop across the channel (i.e., the electrical distance). The profile of the pore has two vestibules which face the bulk solutions. The constriction in the pore indicates a region of high resistance to Ca^{2+} permeation, which presumably separates the vacuolar and cytoplasmic vestibules. The vestibule facing the cytoplasm is deeper and broader than that facing the vacuolar side of the membrane. This is deduced from the stronger voltage dependence of ion block from the cytoplasmic solution found here and by others (e.g., TEA, Homblé and Fuks, 1991; sodium, Bertl, 1989). Sites labeled 1–5 bind divalent ions and sites 6 and 7 bind monovalent ions. The bars attached to the sites indicate the error in estimating the location of these sites. The presence of K^+ sites labeled K are postulated from competition between Ca^{2+} and K^+ from the same side of the membrane. The location of these sites within the pore is unknown. Site 2 is occluded when the external voltage-dependent gate (gate A) is closed (Laver, 1990). The pore conducts K^+ when Ca^{2+} is bound at site 1 but is blocked by Ca^{2+} at the other sites. The external vestibule can be simultaneously occupied by one Ca^{2+} and one K^+ and the cytoplasmic vestibule can bind two Ca^{2+}. Ca^{2+} binds sequentially to sites 3–5 and Ca^{2+} at either site 3 or 4 can lock Ca^{2+} into site 5. External K^+ alleviates Ca^{2+} block at sites 1, 2, 4, and 5 and cytoplasmic K^+ alleviates the block at sites 2–5.

detected. In the channel vestibule facing the cytoplasm Ca^{2+} must bind to either site 3 or 4 before it binds to site 5.

The K^+ channel in *Chara* is a multi-ion channel. Single-ion models for K^+ permeation within the *Chara* K^+ channel (Bertl, 1989; Laver et al., 1989) do not account for the findings of this study. The kinetics of the slow Ca^{2+} block reveals that

two Ca^{2+} can occupy the cytoplasmic vestibule of the channel. The vacuolar vestibule is known to hold only one Ca^{2+} (Laver, 1990). The nature of the competition between divalent and monovalent cations is consistent with the present understanding of ion permeation in K^+ channels; i.e., the maxi-K channel can be occupied by up to four K^+ ions (Neyton and Miller, 1988*b*). Competition between K^+ and Ca^{2+} on the same side of the membrane over a wide range of $[K^+]$ clearly shows the presence of at least two K^+ sites in each channel vestibule. Further, competition between Ca^{2+} and K^+ at opposite ends of the channel shows that one of the cytoplasmic K^+ sites has an equilibrium binding affinity of ~ 10 mM and is located 30% of the way along the trans-pore PD. Similarly it is shown that one of the vacuolar sites has a low affinity (>500 mM) and is superficially located on the protein.

Several lines of evidence indicate that sites 1 and 3 are located on parts of the channel protein that are relatively exposed to the bulk solutions and that sites 2, 4, and 5 are located deep within the pore and are relatively inaccessible: (*1*) The fact that ions binding at sites 2, 4, and 5 must traverse a large fraction of the trans-pore PD suggests a deep location for these sites in the K^+ channel protein. (*2*) Ca^{2+} associates and dissociates from site 5 via either site 3 or 4. (*3*) Binding of divalent ions at sites 2, 4, and 5 is most strongly affected by monovalent ions in the opposite vestibule, suggesting that these sites are in closer proximity to the opposite side of the membrane. Sites 1 and 3, by the same reasoning, must be relatively superficial. (*4*) The high ion specificity of the deep divalent ion binding sites indicates that water has limited access to these sites. The low ion specificity of the superficial sites (sites 1 and 3) is indicative of a well-hydrated, relatively exposed location on the channel protein. (*5*) K^+ and Ca^{2+} are generally less able to cohabit the pore when bound at the deeper sites than at the superficial sites. For example, one K^+ and Ca^{2+} at site 1 are shown to cohabit the vacuolar vestibule, whereas Ca^{2+} at site 4 excludes K^+ from the pore. Also, the binding of Ca^{2+} at site 1 does not totally block K^+ conduction in the channel. This suggests a more confined environment in the vicinity of the deep sites.

I wish to thank Dr. K. A. Fairley for assisting with the experiments, Prof. N. A. Walker and Dr. D. I. Cook for helpful discussions and for critically reading this manuscript, and the referees for their helpful comments.

This work was supported by a Queen Elizabeth II fellowship.

Original version received 11 December 1991 and accepted version received 11 May 1992.

REFERENCES

Bertl, A. 1989. Current-voltage relationships of a sodium-sensitive potassium channel in the tonoplast of *Chara corallina*. *Journal of Membrane Biology*. 109:9–19.

Blatz, A. L., and K. L. Magleby. 1986. Correcting single channel data for missed events. *Biophysical Journal*. 49:967–980.

Draber, S., R. Schultze, and U. Hansen. 1991. Patch-clamp studies on the anomalous mole fraction effect of the K^+-channel in cytoplasmic droplets of *Nitella:* an attempt to distinguish between a multi-ion single-file pore and an enzyme kinetic model with lazy state. *Journal of Membrane Biology*. 123:183–190.

Eisenman, G. 1961. On the elementary atomic origin of equilibrium ionic specificity. *In* Symposium on Membrane Transport and Metabolism. A. Kleinzeller and A. Kotlyk, editors. Academic Press, New York. 163–179.

Eisenman, G., and J. A. Dani. 1987. An introduction to molecular architecture and permeability of ion channels. *Annual Review of Biophysics and Biophysical Chemistry.* 16:205–226.

Ferguson, W. B. 1991. Competitive Mg^{2+} block of a large-conductance, Ca^{2+}-activated K^+ channel in rat skeletal muscle. Ca^{2+}, Sr^{2+}, and Ni^{2+} also block. *Journal of General Physiology.* 98:163–181.

Homblé, F., and B. Fuks. 1991. Quantitative analysis of singe K^+ channels in the tonoplast of Chara corallina: selectivity and TEA blockade. *Journal of Plant Physiology.* 137:729–733.

Kamiya, N., and K. Kuroda. 1957. Cell operation in *Nitella.* I. Cell amputation and effusion of the endoplasm. *Proceedings of the Japanese Academy.* 33:149–152.

Latorre, R., and C. Miller. 1983. Conduction and selectivity in potassium channels. *Journal of Membrane Biology.* 71:11–30.

Laüger, P. 1976. Diffusion-limited ion flow through pores. *Biochimica et Biophysica Acta.* 455:493–509.

Laver, D. R. 1990. Coupling of K^+-gating and permeation with Ca^{++} block in the Ca^{++}-activated K^+ channel in *Chara australis. Journal of Membrane Biology.* 118:55–67.

Laver, D. R., K. A. Fairley, and N. A. Walker. 1989. Ion permeation in a K^+ channel in *Chara australis:* direct evidence for diffusion limitation of ion flow in a maxi-K channel. *Journal of Membrane Biology.* 108:153–164.

Laver, D. R., and N. A. Walker. 1987. Steady-state voltage-dependent gating and conduction kinetics of single K^+ channels in the membrane of cytoplasmic drops of *Chara australis. Journal of Membrane Biology.* 100:31–42.

Laver, D. R., and N. A. Walker. 1991. Activation by Ca^{2+} and block by divalent ions of the K^+ channel in the membrane of cytoplasmic drops from *Chara australis. Journal of Membrane Biology.* 120:131–139.

Liu, Q.-Y., and H. C. Strauss. 1991. Blockade of cardiac sarcoplasmic reticulum K^+ channel by Ca^{2+}. Two-binding-site model of blockade. *Biophysical Journal.* 60:198–203.

Lühring, H. 1986. Recording of single K^+ channels in the membrane of cytoplasmic drop of *Chara australis. Protoplasma.* 133:19–27.

MacKinnon, R., R. Latorre, and C. Miller. 1989. Role of electrostatics in the operation of a high-conductance Ca^{2+}-activated K^+ channel. *Biochemistry.* 28:8092–8099.

Margolis, M. J. 1966. Chemical Principles in Calculation of Ionic Equilibria. Macmillan Publishing Co., New York. 270.

Moczydlowski, E., O. Alvarez, C. Vergara, and R. Latorre. 1985. Effect of phospholipid surface charge on the conductance and gating of a Ca^{2+}-activated channel in plannar lipid bilayers. *Journal of Membrane Biology.* 83:273–282.

Neyton, J., and C. Miller. 1988*a*. Potassium block barium permeation through the high conductance Ca^{2+}-activated K^+ channel. *Journal of General Physiology.* 92:549–567.

Neyton, J., and C. Miller. 1988*b*. Discrete Ba^{2+} block as a probe of ion occupancy and pore structure in the high-conductance Ca^{2+}-activated K^+ channel. *Journal of General Physiology.* 92:569–586.

Oberhauser, A., O. Alvarez, and R. Latorre. 1988. Activation by divalent cation of a Ca^{2+}-activated K^+ channel from skeletal muscle membrane. *Journal of General Physiology.* 92:67–86.

Sakano, K., and M. Tazawa. 1986. Tonoplast origin of the membrane of cytoplasmic droplets prepared from *Chara* internodal cells. *Protoplasma.* 131:247–249.

Truesdell, A. H., and C. L. Christ. 1967. Glass electrodes for calcium and other divalent cations. *In* Glass Electrodes for Hydrogen and Other Cations. G. Eisenman, editor. Marcel Dekker, Inc., New York. 293–321.

Tyerman, S. D., B. R. Terry, and G. P. Findlay. 1992. Multiple conductances in the large K^+ channel from *Chara coralina* shown by a transient analysis method. *Biophysical Journal.* 61:736–749.

Vergara, C., and R. Latorre. 1983. Kinetics of Ca^{2+}-activated K^+ channels from rabit muscle incorporated into planar lipid bilayers. Evidence for Ca^{2+} and Ba^{2+} blockade. *Journal of General Physiology.* 82:543–568.

Villarroel, A., and G. Eisenman. 1989. Ca^{2+} block in the large Ca^{++}-activated K^+ channel. An estimate of the surface charge of the internal vestibule. *Biophysical Journal.* 55:7*a*. (Abstr.)

Vivaudou, M. B., J. J. Singer, and J. V. Walsh, Jr. 1986. An automated technique for analysis of current transitions in multi-level single-channel recordings. *Pflügers Archiv.* 407:355–364.

Woodhull, A. M. 1973. Ionic blockage of sodium channels in nerve. *Journal of General Physiology.* 61:687–708.